Journal of Applied Catalysis and Engineering

https://doi.org/10.17756/acce.2021-006

Review article

Open Access

# A Review on the Modification Strategies of TiO2 Photocatalyst Coatings

**Sujun Guan[1*], Liang Hao[2] and Yun Lu[3]**

[1]*Bio-Nano Electronics Research Centre, Toyo University, Saitama, Japan*

[2]*College of Mechanical Engineering, Tianjin University of Science and Technology, Tianjin, China*

[3]*Department of Mechanical Engineering, Chiba University, Chiba, Japan*

**[*]Correspondence to:**
Sujun Guan
Bio-Nano Electronics Research Centre
Toyo University
Saitama 350-8585, Japan.
**Tel:** 81-492391940
**E-mail:** guansujun1222@gmail.com

**Received:** May 31, 2021
**Accepted:** July 11, 2021
**Published:** July 12, 2021

**Citation:** Guan S, Hao L, Lu Y. 2021. A Review on the Modification Strategies of $TiO_2$ Photocatalyst Coatings. *J Appl Cat Chem Eng* 2(1): 1-21.

**Copyright:** © 2021 Guan et al. This is an Open Access article distributed under the terms of the Creative Commons Attribution 4.0 International License (CC-BY) (http://creativecommons.org/licenses/by/4.0/) which permits commercial use, including reproduction, adaptation, and distribution of the article provided the original author and source are credited.

Published by United Scientific Group

## Abstract

In recent years, $TiO_2$ photocatalysis has received much research interest owing to its potential applications in the field of environmental remediation. However, the large bandgap of $TiO_2$ and fast recombination of photogenerated charge carriers limit its overall photocatalytic efficiency. The large bandgap of $TiO_2$ can be narrowed by modifying the electronic band structure, such as doping elements, forming oxygen vacancies. The fast recombination can be corrected by changing the effect of charge transfer, including the addition of suitable electron acceptors, heterojunction, Z-scheme. This brief review mainly describes the principal results of modification strategies on the $TiO_2$ photocatalyst coatings formed on $Al_2O_3$ balls. The modification strategies encompass porous structure, nano-surface, carbon-doping, combination with TiC and graphene oxide. It is expected that the insights of this up-to-date review could guide the synergistic modification strategies to improve the performance of $TiO_2$ photocatalyst coatings to achieve their maximum potentials.

## Keywords

$TiO_2$ photocatalyst; Modification strategies; Porous structure; Nano-surface; Carbon-doping; Charge transfer; Photocatalytic activity

## Introduction

TThe supply and use of energy are related not only to global warming, but also to environmental problems, such as air pollution, wastewater, forest destruction, and emission of radioactive substances. Recently, environmental problems have extended to the control of air pollutants, such as hazardous chemical substances and harmful in small doses, as well as to that of globally significant pollutants [1-3]. According to the potential solutions, numerous attempts have been made to develop photocatalysts that work not only under UV light but also visible light illumination to efficiently utilize solar energy.

Photocatalyst has recently become a well-known word and various materials using photocatalytic functions have been commercialized [4-8]. Among the available photocatalyst of $TiO_2$, ZnO, $SrTiO_3$, $CeO_2$, $WO_3$, CdS and ZnS, $TiO_2$ has been considered as few of the most promising photocatalysts for the potential material in environment purification, sterilization, self-cleaning surfaces, and hydrogen generation due to its high photocatalytic activity, excellent chemical stability, non-toxicity, and low cost [9-12]. Since the report of the water splitting using a $TiO_2$ electrode under an anodic bias potential from Honda and Fujishima [4], there are many researchers have been intensively devoted to the development

of photocatalytic materials, with utilizing solar energy and thus solving the increasing global problems of environmental remediation and clean fuel production. It is well-known that the reaction processes during $TiO_2$ are as follows. i) the electrons and holes will be separated after absorbing the necessary energy, ii) some of the electrons are raised into the conduction band leaving holes in the valence band, iii) some of the electrons and holes reach the surface to react with the attached organic matter. From the reaction processes of $TiO_2$, it could be easy to understand that the photocatalytic activity of $TiO_2$ towards a specific reaction depends on both its properties and external conditions. Properties such as the surface morphology, particle size, specific surface area, crystal structures highly influence the photocatalytic activity. The external conditions involve the intensity of the light irradiation, the pH of the reaction system, and so on. These factors often interactively influence photocatalytic activity [13].

Currently, $TiO_2$ has two major drawbacks, consisting in its relatively large energy band gap (3.2 eV for the anatase, 3.0 eV for the rutile), which hampers the exploitation of solar light in photocatalytic reactions, and the high recombination of the photogenerated electron-hole pairs [9-13]. Various strategies to enhance the photocatalytic activity of $TiO_2$, as shown in figure 1, including the modification of crystal phase [14-16], regulation of electronic structure [17-19], surface sensitization and modification of semiconductor [20-22], interfacial heterojunctions [23-26], have been developed to modify the reaction processes, such as involving light-harvesting and excitation, as well as surface trapping and charge transfer.

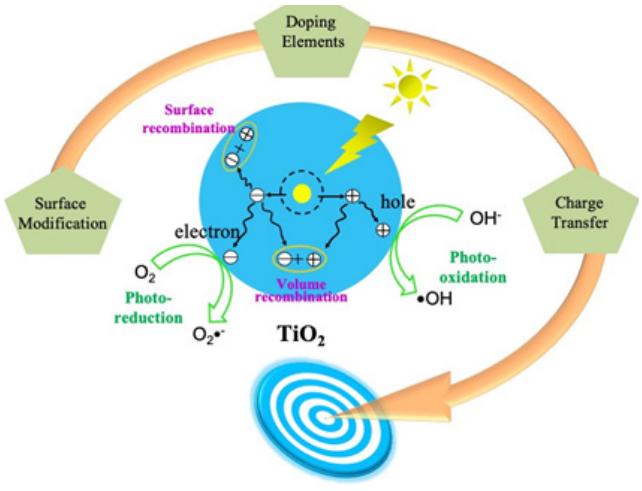



**Figure 1:** Schematic diagram of the modification strategies of TiO2 photocatalyst.

This review is to mainly summary the principal results of modification strategies on the $TiO_2$ photocatalyst coatings formed on $Al_2O_3$ ball by mechanical coating technique (MCT), owing to the mechanical strength of $Al_2O_3$ ball for the formation during the MCT and its low-cost. We have attempted various modification strategies, encompassing the increased surface accessible area, narrowed band gap and effect of charge transfer. By grouping the modification steps of porous structure and nano-surface, carbon-doping and K-doping, charge transfer via the combination with graphene oxide as well as Ti coatings are revealed. Further, this review attempts to provide the synergistic modification strategies to improve the performance of $TiO_2$ photocatalyst coatings to achieve their maximum potentials.

## $TiO_2$ photocatalyst coatings by regular process

### Fabrication of $TiO_2$ photocatalyst coatings

The schematic diagram of the MCT and following heat treatment (HT) process is shown in figure 2. Ti powder (purity of 99.1%, average diameter of 30 μm) was used as coating materials, and $Al_2O_3$ balls (purity of 93.0%, average diameter of 1 mm) were used as substrates materials. Ti powder and $Al_2O_3$ balls were put into the alumina bowl with a volume of 250 mL (dimensions of Φ 75 mm × 70 mm). The milling operation was carried out for 10 h, with a 10-minute milling operation followed by a 2-minute cooling interval to avoid excessive heating of the bowl. The MCT was fixed at 480 rpm (revolutions per minute) for 10 h, named "Ti coatings". The detailed MCT process could be found in our previous work [27-29].

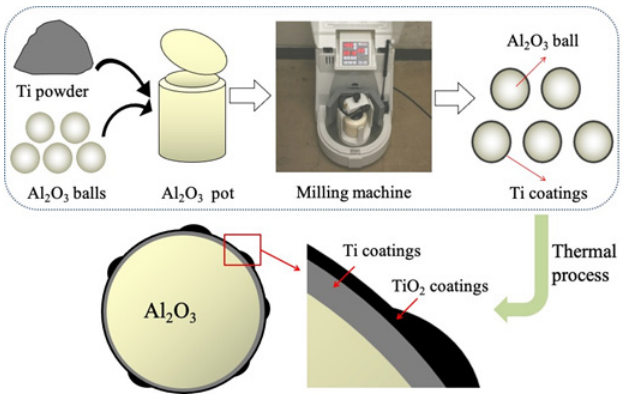



**Figure 2:** Schematic fabrication diagram by MCT and HT process.

Figure 3 shows the schematic set of Ti coatings were then fabricated by HT in the air using an electric furnace (HPM-1G, As one, Japan), with a series of relatively low temperatures

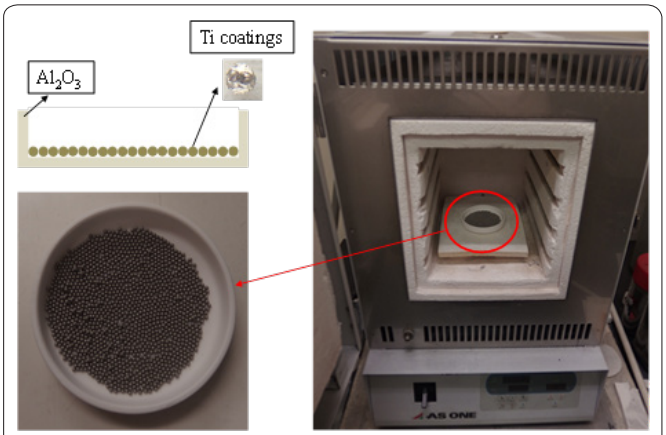



**Figure 3:** Schematic set of Ti coatings by HT in the air using an electric furnace.

of x (873 K, 937 K, and 1073) K for y (3 h, 10 h, and 15) h. Then, the samples cooled to room temperature in the furnace, and were named "Air-xKyh". The samples were treated by ultrasonic cleaning (frequency: 40 kHz) in acetone for 15 min to remove any substances that did not strongly adhere to the surfaces .

## Characterization

The formed compounds of the prepared samples were analyzed using X-ray diffraction (XRD, D8 Advance, Germany) equipped with Cu-Kα radiation at 40 kV and 40 mA, at a scanning rate of 0.02° s-1. The surface morphology was examined by scanning electron microscopy (SEM, JSM-5300). The O 1s and Ti 2p were analyzed by X-ray photoelectron spectroscopy (XPS, ESCALAB 250Xi, Thermo, US). The ultraviolet-visible absorption spectra of the prepared samples were measured by an ultraviolet-visible spectrophotometer (UV-vis, Model MSV-370, Jasco, Japan) with a wavelength range of 370-700 nm. Photoluminescence emission and excitation were obtained with a fluorometer (PL, F-4600) with an excitation wavelength of 465 nm.

According to the ISO 10678-2010, the photocatalytic activity was evaluated by measuring the degradation rate of methylene blue (MB) solution (C0: 10 μmol/L, 35 mL) under UV and visible light irradiation at room temperature. The photocatalytic reactor system schematically is shown in figure 4.

The evaluation process of photocatalytic activity of the

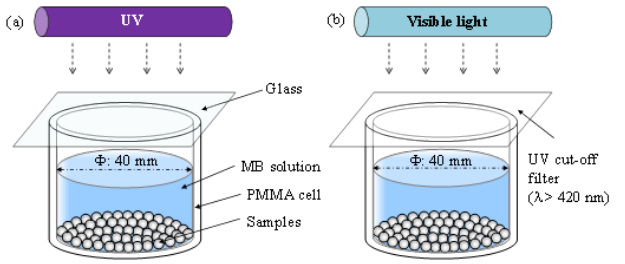



**Figure 4:** Schematic diagram of the photodecomposition reactor system according to ISO 10678-2010. (a) Under UV irradiation, (b) Under visible light irradiation.

samples can be divided into three steps (Figure 5). Firstly, the prepared samples were dried under UV light (FL20S BLB, Toshiba) for 24 h, and adsorption of MB solution (20 μmol/L, 35 mL) was carried out in the dark for 18 h. Two 20 W fluorescent lamps (NEC FL20SSW/18) were used as the irradiation source (irradiance of 5000 lx), and a UV cut-off filter (L42, Hoya) was used to ensure that only visible light (λ > 420 nm) could reach the samples. The degradation rate constant (k, nmol L-1 min-1) of MB solution concentration versus irradiation time was calculated by the least-squares method with the

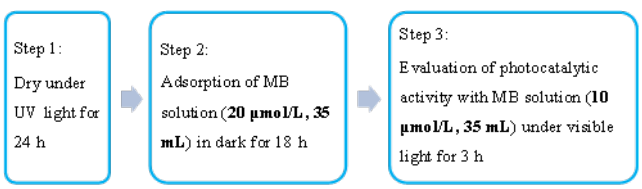



**Figure 5:** The evaluation process of photocatalytic activity of the samples with three steps.

data. To clearly show the photocatalytic activity of samples, here use R-value to describe the difference of the degradation rate constants k. R is calculated by the following equation:

$$R = k_{sample} - k_{MB} \quad (1)$$

where, kMB is to describe the degradation rate constants of MB solution without samples. To establish the stability of the photocatalytic activity, tests were carried out in cycles. Once a testing cycle was completed, the next cycle began after fresh MB solution adsorbed to ensure an initial concentration of ~10 μmol/L.

## Results and Discussion

TAppearance. After HT in air with various conditions, the Air-xK15h samples appear various colors, as shown in figure 6. With extending the HT time at 873 K, the color of the Air-873Kyh samples shows grey, almost without any change. While extending the HT time at 973 K, the color of the Air-973Kyh samples changes from brown (Air-973K3h) to dark-blue (Air-973K10h) and then light-blue (Air-973K15h). While extending the HT time at 1073 K, the color of the Air-1073Kyh samples changes from grey (Air-1073K3h) to dark-white (Air-1073K10h) and light-white (Air-1073K15h). The difference in color between the samples could be related to the band gap, owing to the different crystal structure [26].




**Figure 6:** Appearance of the Air-xKyh samples fabricated by HT in air.

Formed compounds. Figure 7 shows XRD patterns of the Air-xKyh samples fabricated by HT in the air for Ti coatings. The influence of HT temperature on the formed compounds of the Air-xK15h samples is obvious. From Ti coatings, the diffraction peaks at 35.1°, 38.3°, 40.1°, 52.9°, and 62.9° could be well indexed to the (100), (002), (101), (102), and (110) crystal planes of Ti. After HT in the air at 1073 K for 15 h, the Air-1073K15h sample clearly shows that the diffraction peaks at 27.4°, 36.1°, 41.2°, and 54.3°, which could be well indexed to the (110), (101), (111), and (211) crystal planes of rutile TiO2 (JCPDS # 21-1272). In the case of HT in the air at 873 K, figure 7a shows the influence of HT time on the formed compounds of the Air-873Kyh samples is slight.

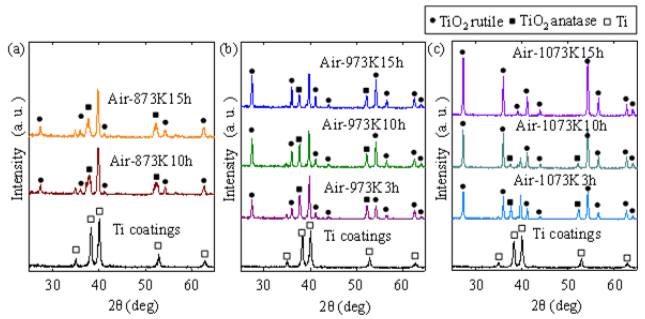



**Figure 7:** XRD patterns of the Air-xK15h samples fabricated by HT in air.

Moreover, the Air-873K15h sample shows the main peaks are from Ti and a slight mixed-phase of rutile $TiO_2$ and anatase $TiO_2$. While after HT in the air at 973 K, the relative intensity of rutile increased with extending the HT time from 3 h to 15 h. With extending the HT time from 3 h to 15 h at 1073 K, the peaks of anatase transferred to that of rutile, and Ti peaks disappeared. For further comparison, the mass fraction of rutile (XR) was calculated from the respective peak intensities using the following equation [30]:

$$XR\ (\%) = \{1 - (1 + 1.26\ IR/IA)-1\} \times 100 \qquad (2)$$

where IR and IA are X-ray intensities of the rutile (110) and anatase (004) peaks, respectively. From table 1, it could clearly find that the influence of the HT conditions on the XR is obvious, especially affected by the temperature.

**Table 1:** $X_R$ of the Air-*x*Kyh samples fabricated by HT in air.

| **Air-*x*Kyh** | $X_R$ |
|---|---|
| Air-873K10h | 0.4 |
| Air-873K15h | 0.41 |
| Air-973K3h | 0.5 |
| Air-973K10h | 0.6 |
| Air-973K15h | 0.76 |
| Air-1073K3h | 0.91 |
| Air-1073K10h | 0.95 |
| Air-1073K15h | 0.98 |

Morphology evolution. Figure 8 shows the surface morphology of Air-xKyh samples, compared with extending the HT times at each temperature. Compared with Ti coatings, the formed compounds were found from the Air-873Kyh samples, but the surface morphology did not show obvious change with extending the HT time at 873 K. While extending the HT time at 973 K, the formed compounds increase in number and size. The structure grows to the needle-like structure at 973 K. Moreover, extending the HT time at 1073 K, the formed compounds show the needle-like structure at 1073 K for 3 h and 10 h and grow to the columnar-like structure at 1073 K for 15 h. Comprehensive consideration of the phase transformation and the changes of surface microstructure, it could conclude that the phase transformation from anatase to rutile effected by the surface morphology [31, 32].

Figure 9 shows the cross-sections of Air-xKyh samples. The oxidized layer is too thin to be detected from the Air-873Kyh

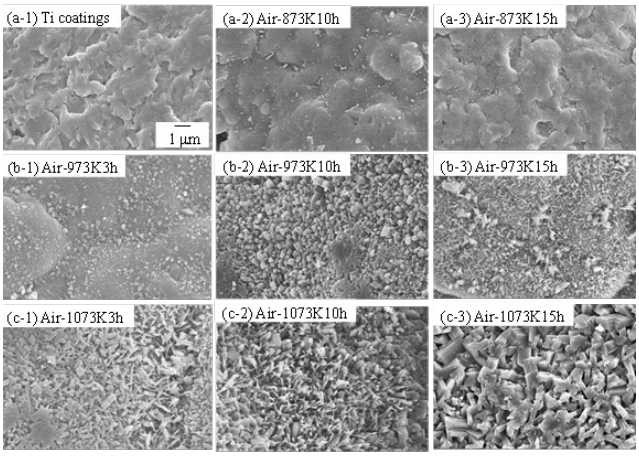



**Figure 8:** SEM images of surfaces of the Air-xKyh samples fabricated by HT in air. The scale of each image is 1 μm. (a) 873 K, (b) 973 K, (c) 1073 K.

samples. When heat treatment in air at 973 K, a thin oxidized layer could be detected until extending the time to 15 h, with a 2-μm thin oxidized layer, as shown in figure 9b. When heat treatment in air at 1073 K, the layer grows to be more obvious, and the thickness of the oxidized layer increases from about 3 μm of the Air-1073K3h sample to 18 μm of the Air-1073K15h sample. Compared with the influence of HT time, the influence of HT temperature on the growth of the oxidized layer is more obvious. The change hints that the HT temperature could significantly accelerate the growth of the oxidized layer.

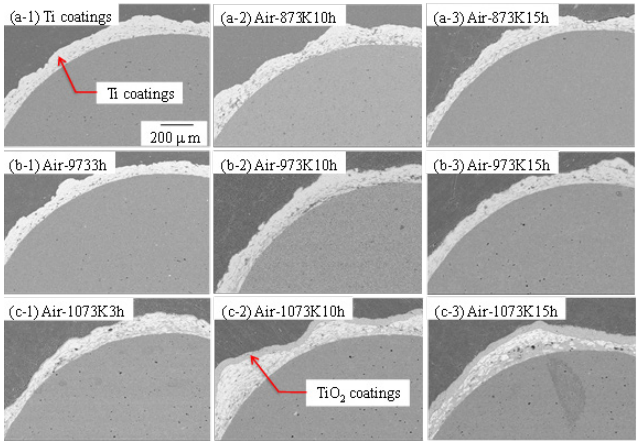



**Figure 9:** SEM images of cross-sections of the Air-xKyh samples fabricated by HT in air. (a) 873 K, (b) 973 K, (c) 1073 K. The scale of each image is 200 μm.

Photocatalytic activity. The photocatalytic activity of the Air-xK15h samples has been investigated by degradation of MB solution under UV irradiation, as shown in figure 10 and 11 clearly shows the degradation rate constant of the photocatalytic activity with different HT conditions. From figure 10, it is evident that the concentration of the dashed line (marked with MB solution) hardly decreased, which hints the MB solution did not degrade. The concentration of the Ti coatings slightly increases because there is some content of desorption after the adsorption in dark for 18 h with a higher concentration of MB solution during step 2. In general, all samples show photocatalytic activity. While from figure 11,

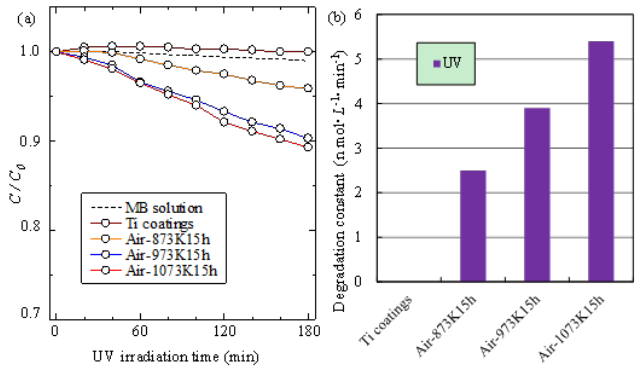



**Figure 10:** Comparison of the photocatalytic activity of the Air-xK15h samples. (a) Degradation of MB solution by different samples, (b) Degradation constant rate. μm.

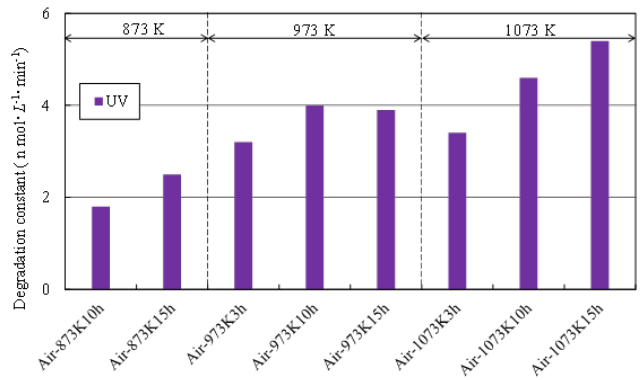



**Figure 11:** Degradation constant rate of the photocatalytic activity of the Air-xKyh samples fabricated by HT in the air.

it could draw that the trend of photocatalytic activity of the Air-xKyh samples increases, with increasing the HT time at each HT temperature. Compared with the influence of HT time at each HT temperature, the HT temperature plays a more important role in the enhancement of the photocatalytic activity of the Air-xKyh samples. The enhanced photocatalytic activity is widely considered to the efficiency of charge transfer [33-35]. When $TiO_2$ contacts with a metal with a higher work function, the photogenerated electrons in the CB of $TiO_2$ may transfer to the metal, which could suppress the recombination between the pairs of electron and hole in $TiO_2$, thereby enhancing the photocatalytic activity.

## Modification strategy of sulfuric-acid-bath treatment

It is well-known that nanomaterials have become pioneering photocatalysts and account for most of the current research in the photocatalysis area. In general, nanomaterials are with properties beneficial to photocatalysis, owing to the large surface areas, abundant surface states, diverse morphologies, and easy device modeling [36-42]. Significant progress has been made in the development of novel nanomaterials on the efficiency, especially in visible-light response photocatalysis to meet engineering requirements. The catalytic properties of $TiO_2$ can be altered by the surface structure, due to the surface absorption effect and photoabsorption. Numerous reports have shown that the nanostructured surface, especially porous surface, plays an important role in the photocatalytic activity of $TiO_2$ [40, 43-45].

### Sulfuric-acid-bath treatment (SAT) for Ti coatings

In this part, we proposed an approach to fabricate the $TiO_2$ photocatalyst coatings with porous structure, by the SAT followed by soaking in sulfuric acid (SA) at room temperature then oxidation in the air, as shown in figure 12. Firstly, Ti

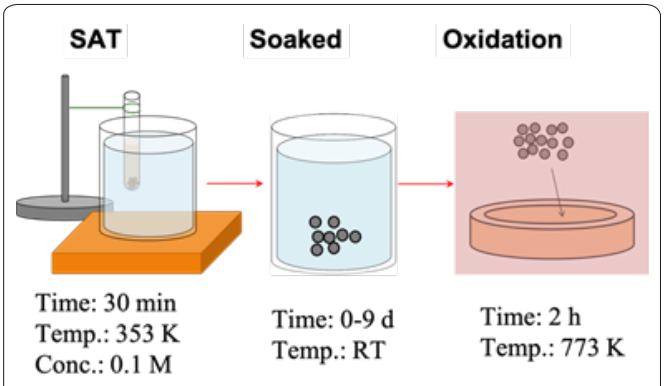



**Figure 12:** Schematic process of SAT for Ti coatings

coatings were coated on $Al_2O_3$ balls by MCT, using Ti powder. The formed Ti coatings were then exposed in sulfuric-acid-bath treatment (SAT) in H2SO4 (0.1 and 1.0 M) at 80 °C for 30 and 60 min and named as "xSAy", with x being the SA concentration and y being the SAT time. Then, the xSAy samples were soaked in SA of 1.0 M at room temperature for a variable time duration and named "xSAy-zd", with z being the soaked time. Finally, the xSAy-zd samples were oxidized in the air using an electric furnace at 773 K for 2 h, and named as "xSAy-zd-O".

The influence of the SAT and soaked conditions on the surface morphology and photocatalytic activity of $TiO_2$ coatings was studied and the relationship among the change of photocatalytic activity and the surface morphology, mixed-phase of anatase and rutile, as well as formed hydroxyl groups was discussed.

### Appearance of SA during SAT

Figure 13 shows the appearance of SA changes during SAT with different SA concentrations, for Ti coatings at 80 °C at different times. With extending the SAT time to a relatively lower concentration of 0.1 M (Figure 13a), it is hard to find the color changes, which hints that the reaction between Ti and H2SO4 solution is difficult. While from figure 13b with increasing the concentration to 1.0 M, it clearly shows that the color changes from colorless to purple with 20 min, then black at 30 min. The difference in the appearance during SAT with different SA concentrations hints that the formed nucleation of $TiO_6$ octahedra [46, 47], during the reaction between Ti and $H_2SO_4$ solution is more responsive, with relative higher SA concentration. .

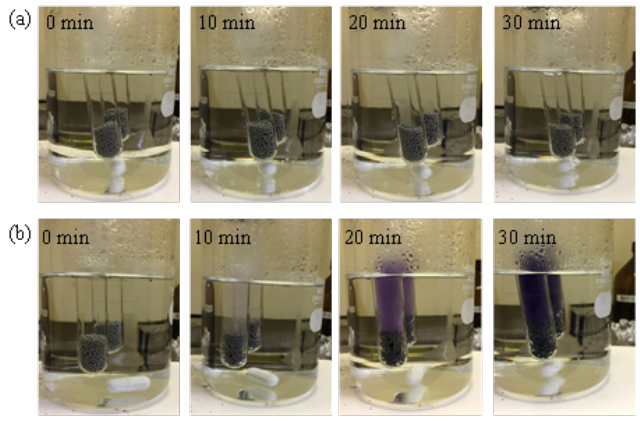



**Figure 13:** The appearance of sulfuric acid during SAT at 80 °C for a different time, in different SA concentrations. (a) 0.1 M, (b) 1 M.

## Surface evolution

The influence of the SAT and soaked conditions on the surface morphology of the xSAy-zd-O samples after oxidation in the air is shown in figures 14-16. Compared with that without SAT [48], Figure 14b shows a little effect on the change in surface morphology, which also reveals that the reaction between Ti and a relatively lower concentration of H2SO4 solution has hardly occurred. With extending the soaked time from 0 day to 9 days, it clearly shows the change in surface morphology, such as the crack in figure 14f. Then increasing the SA concentration from 0.1 M to 1.0 M, the influence of the SA concentration and soaking time on surface morphology is obvious. Figure 15b clearly shows the porous-like structure formation on the surface of Ti coatings, as shown in red arrow. It means that increasing the SA concentration is an effective method to promote the reaction between Ti and $H_2SO_4$. With extending the soaked time from 0 day to 9 days, the formed porous-like structure becomes too few and disappears. While extending the SAT time from 30 min to 60 min, it also clearly shows the porous-like structure forms on the surface of Ti coatings, and the size of the porous-like structure becomes larger (Figure 16b). Similarly, the formed porous-like structure becomes too few and disappears, with extending the soaked time from 0 day to 9 days. A comprehensive comparison of the influence of the SAP and soaked conditions on the surface morphology of the 1.0SAy-zd-O samples, we can conclude that the reaction between Ti and $H_2SO_4$ continues during the soaking process and the outside of Ti coatings might become shedding when the soaking time is higher than 5 days.

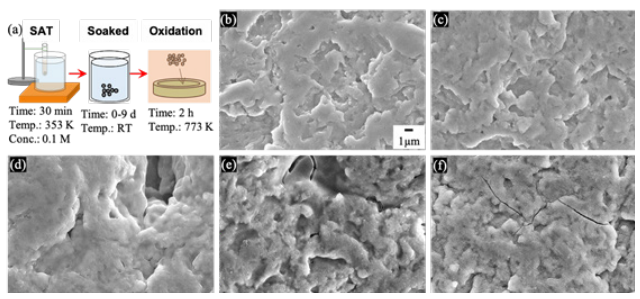



**Figure 14:** Schematic process (a) and surface morphology of the 0.1SA30-zd-O samples. (b) 0 day, (c) 3 days, (d) 5 days, (e) 7 days, (f) 9 days. The scale in the image from b-f is 1 μm.

## Formed compounds

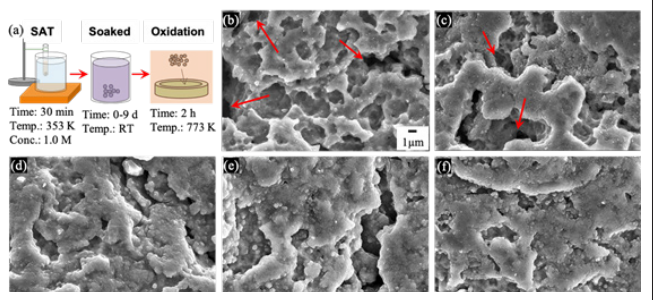



**Figure 15:** Schematic process (a) and surface morphology of the 1.0SA30-zd-O samples. (b) 0 day, (c) 3 days, (d) 5 days, (e) 7 days, (f) 9 days. The scale in the image from b-f is 1 μm.

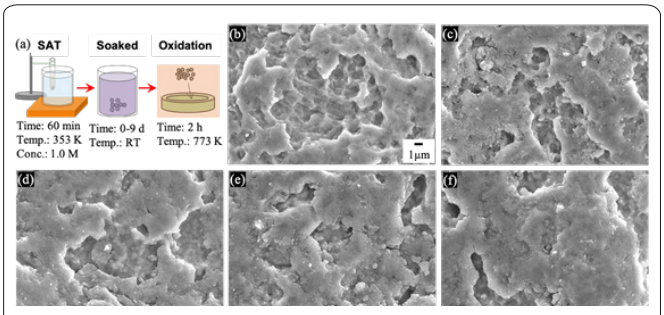



**Figure 16:** Schematic process (a) and surface morphology of the 1.0SA60-zd-O samples. (b) 0 day, (c) 3 days, (d) 5 days, (e) 7 days, (f) 9 days. The scale in the image from b-f is 1 μm.

To investigate the formed compounds on Ti coatings, Raman spectroscopy of the xSAy-zd-O samples is shown in figure 17. For comparison, Raman spectroscopy of $TiO_2$ anatase (red line) and $TiO_2$ rutile (blue line) has also been presented. Also, the XRD results show that the formed $TiO_2$ on Ti coatings is mainly in the form of anatase during oxidation in air at 773 K (Figure 18). While changing the SA conditions, XRD results of the samples hardly show any change. In general, compared with the peaks of anatase and rutile, the only peak at 428 cm-1 of all samples shows the shift, as shown by light-blue frame, which hints that the mixed-phase of anatase and rutile has formed, similarly to the previous reported [49-51]. For the 0.1SA30-zd-O samples, it shows that the main peak is anatase at 146 cm-1. While increasing the SA concentration from 0.1 M to 1.0 M, the main peak changes from anatase at 146 cm-1 to rutile at 428 cm-1 and 612 cm-1. Also, by extending the

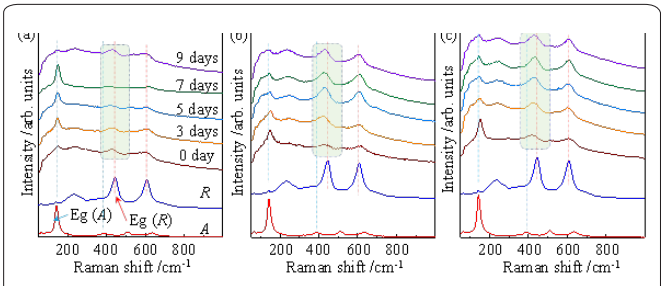



**Figure 17:** Raman spectroscopy of the xSAy-zd-O samples. (a) 0.1SA30-zd-O, (b) 1.0SA30-zd-O, (c) 1.0SA60-zd-O. A is anatase, R is rutile.

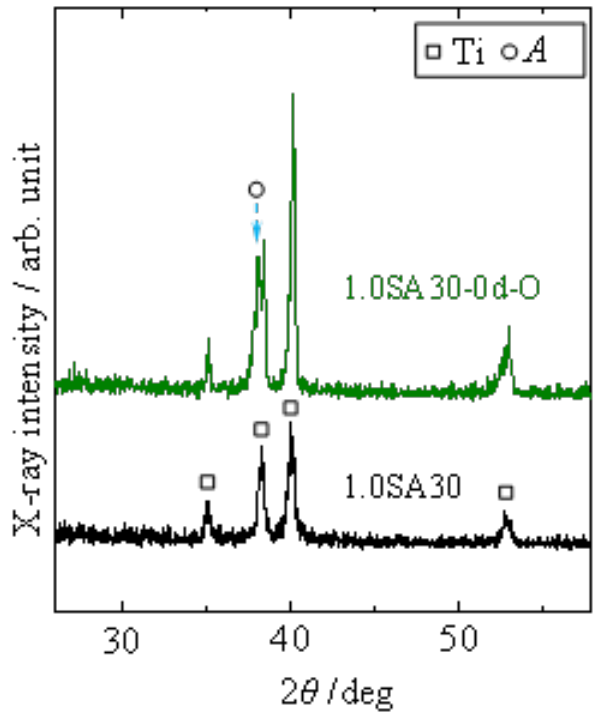



**Figure 18:** X-ray patterns of the 1.0SA30 and 1.0SA30-0d-O samples.

soaked time from 0 day to 9 days, figures 17b and 17c show the phase transformation and the mixed-phase. Raman results have also confirmed that increasing the SA concentration and extending the soaked time are effective methods to promote the reaction between Ti and $H_2SO_4$.

## Photocatalytic activity

The photocatalytic activity of the xSAy-zd-O samples was evaluated by the degradation of MB solution at room temperature, as shown in figure 19. From figure 19a-c, the concentration of MB indicated by the dashed line (marked as MB) hardly decreased, which hints the MB solution does not degrade by itself under UV irradiation. Compared with that of MB solution, all samples show photocatalytic activity, according to the concentration changes of MB solution. For the 0.1SA30-zd-O samples, the influence of the soaking time on photocatalytic activity is obvious. While increasing the SA concentration from 0.1 M to 1.0 M, figures 19b and 19c show the influence of the soaking time is similar and the photocatalytic activity has been relatively enhanced, compared with that of the 0.1SA30-zd-O samples. In general, with extending the soaked time from 0 day to 9 days, figure 19d clearly shows the degradation rate constants of the xSAy-zd-O samples first increases then decreases, reaching the highest with 7 days, which could be considered to the phase transformation and the mixed phase (Figure 17). The enhancement of the xSAy-zd-O samples on photocatalytic activity is remarkable, which could be related to the mixed-phase of anatase and rutile [52, 53], and the changed accessible surface area via the surface structure [54, 55]. Comprehensive consideration of cost and photocatalytic activity of the xSAy-zd-O samples, it can be concluded that the best fabrication condition is SAP in 1.0 M of $H_2SO_4$ solution for 30 min followed soaked 7 days then oxidation in air for Ti coatings among the conditions tested.

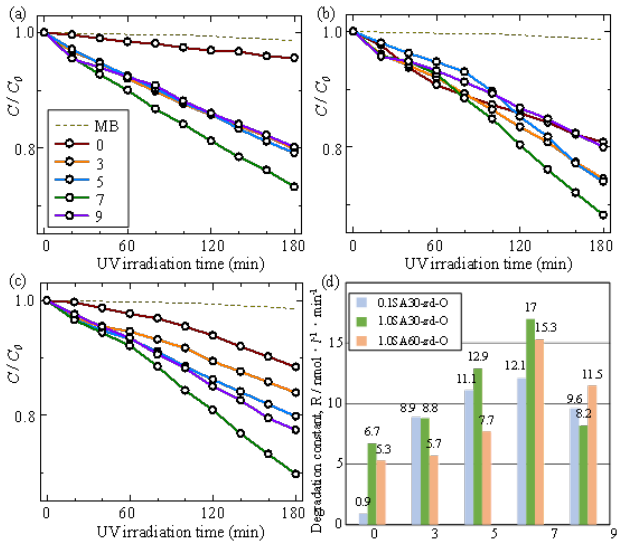



**Figure 19:** Comparison of the photocatalytic activity of the xSAy-zd-O samples. (a) 0.1SA30-zd-O, (b) 1.0SA30-zd-O, (c) 1.0SA60-zd-O, (d) Degradation constant rate.

## XPS analysis

Based on the highest photocatalytic activity of the 1.0SA30-7d-O sample, XPS has been used to gain insight into the surface chemical bonding of the 1.0SA30-0d-O and 1.0SA30-7d-O samples, as shown in figure 20. From figures 20a and 20b, it could find that the main spectra of C 1s and Ti 2p are with the typical peaks for the two samples, respectively.

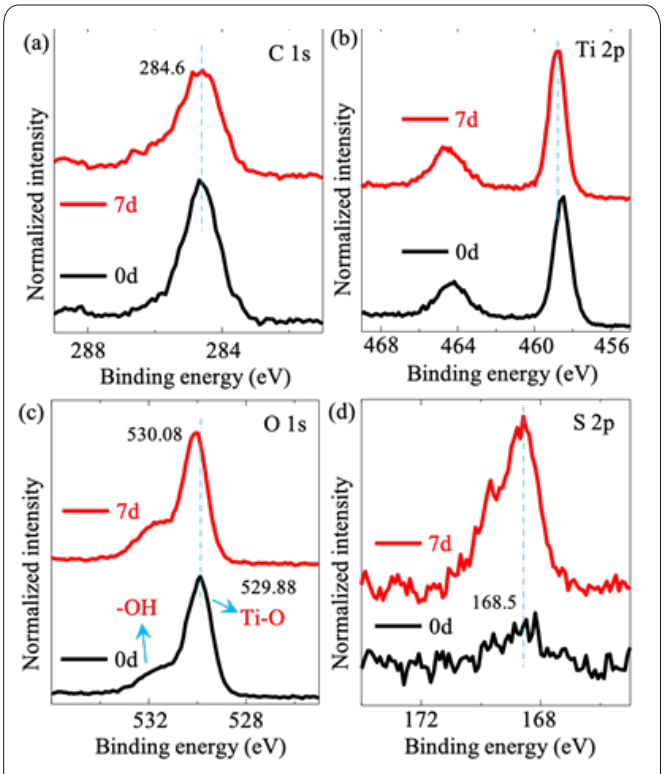



**Figure 20:** XPS spectra of the 1.0SA30-zd-O samples. (a) C 1s, (b) Ti 2p, (c) O 1s, (d) S 2p.

Notably, from figure 20c, with extending the soaking time, it is found that the slight shift of O 1s peak, which would be related to the phase transformation from anatase with 3.2 eV and rutile with 3.0 eV [52, 53]. While figure 20c also shows the change of the formed hydroxyl groups, the relative content of hydroxyl groups increased with a longer soak time. It is known that the peak shift and the formed hydroxyl groups are due to the influence of the reaction between Ti and $H_2SO_4$, which is favored to enhance photocatalytic performance, similar to the previous reports [56, 57]. Meanwhile, with a longer soaked time, the S 2p peak was also enhanced from the 1.0SA30-7d-O sample, which could confirm the further reaction between Ti and $H_2SO_4$.

## Modification strategy of carbon-embedding heat treatment (cHT)

From figure 1, it is easy to understand the enhancement on photocatalytic activity of photocatalyst TiO2. They focus on two main opinions of narrowing the band gap and suppressing the recombination of the electron-hole pairs [9-13]. In the case of narrowing the band gap, the introduction of a dopant in the $TiO_2$ lattice may affect the electronic band edges or introduce impurity states in the band gap of the system. The doping of $TiO_2$ is currently attracting considerable interest as a promising route to extend the optical absorption of this material to the visible spectral region. This would allow the use of sunlight in photochemistry and photocatalysis, with important and beneficial fallout on the environment and economy. The most widely used approach to enhancement of the photocatalytic activity under the visible region has been doping with metals and more recently non-metallic elements [17, 58, 59]. Among nonmetal elements, nitrogen (N) has been extensively studied in the past few years [17, 60]. Recently, various studies report carbon (C)-doped $TiO_2$ absorption properties in the visible spectrum [16, 61, 62]. The C-doped $TiO_2$ shows a fundamental optical absorption at 535 nm and has a lower band gap of 2.32 eV [58].

Therefore, this part will focus on the enhancement of the photocatalytic activity of photocatalyst coatings via carbon doping and nano-surface structure, by carbon-embedding heat treatment (cHT) for Ti coatings.

### cHT for Ti coatings

TIn this part, we proposed an approach to enhance the photocatalytic activity of $TiO_2$ photocatalyst coatings with carbon doping and nano-surface structure, by cHT in carbon powder (average diameter of 150 μm, purity of 100%) for Ti coatings, as shown in figure 21. Firstly, the formed Ti coatings were heated with the carbon atmosphere at 1073 K for 15 h using an electric furnace, then cooled to room temperature in the furnace, and named "C-1073K15h". For comparison, the Ti coatings were also heat-treated in the air at 1073 K for 15 h and named "Air-1073K15h ".

### Comparison of C-doped $TiO_2$ and $TiO_2$

Appearance and formed compounds. Figure 22 shows the appearance and XRD patterns of the samples of Air-1073K15h and C-1073K15h fabricated by HT in the air and carbon atmosphere, respectively. The color shows brown from the C-1073K15h sample and light-white from the Air-1073K15h sample. After cHT, the diffraction peaks at 36.1°, 42.0°, and 60.9° could be attributed to the (111), (200), and (220) crystal planes of TiCxOy, respectively. Whereas the diffraction peaks at 27.4°, 36.1°, 41.2°, and 54.3° could be well

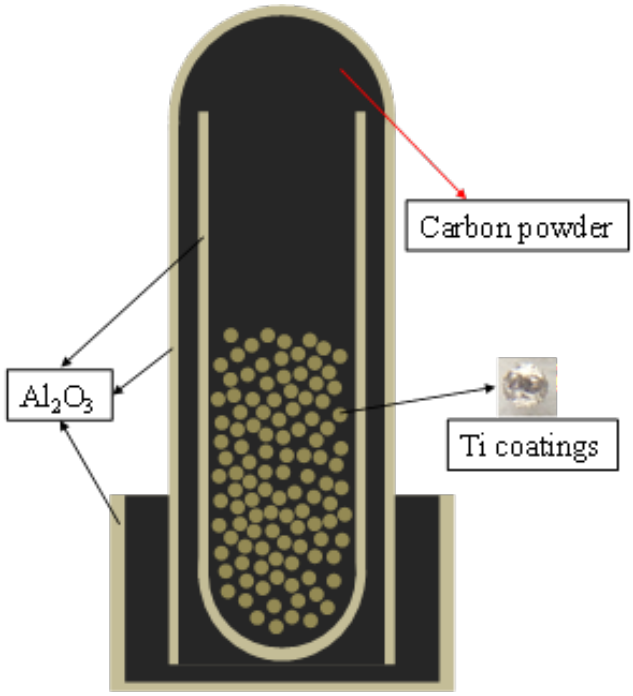



**Figure 21:** Schematic diagram of the set of Ti coatings embedded in carbon powder.

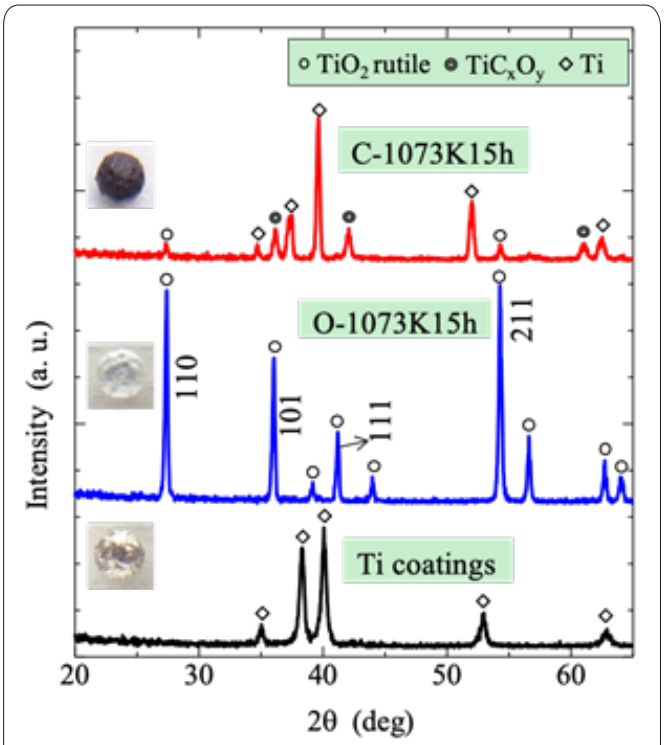



**Figure 22:** Appearance and XRD patterns of the samples fabricated by HT in the air and cHT.

indexed to the (110), (101), (111), and (211) crystal planes of rutile $TiO_2$. It means the C-1073K15h sample is with mixed crystal of TiCxOy and rutile $TiO_2$ forms on the surface of Ti coatings, while the Air-1073K15h sample is with only rutile $TiO_2$. The difference in color between the samples of C-1073K15h and Air-1073K15h could be related to the band gap, owing to the different crystal structure [26].

Morphology evolution. Figure 23 shows the surface morphology of the samples of Air-1073K15h and C-1073K15h. The change of the surface morphology is remarkable, shown the size of surface morphology decreases from micro by HT in the air to nano by cHT. The reason of the change is related with the micro-column structure of the Air-1073K15h sample to the nano-bump structure of the C-1073K15h sample. It is well-known that Ti can easily react with oxygen to form titanium oxide, and the key oxidation process dominating the growth of titanium oxide depends on the predominant diffusion of Ti or oxygen. The predominance of Ti versus oxygen diffusion is influenced by the oxygen concentration, which would affect the structure of titanium oxide [64, 65]. During the HT in the air, the enough amount of oxygen makes oxygen diffusion to be predominant, to form rutile $TiO_2$ with the micro-column structure. While during the cHT, the TiCxOy is formed by the reaction of Ti, oxygen and carbon, and the carbon atmosphere would cause the reaction process to occur under a relatively low oxygen concentration [64]. Hence, the significant change of surface morphology could be considered as the difference in the crystal structure and the predominant diffusion of Ti and oxygen.

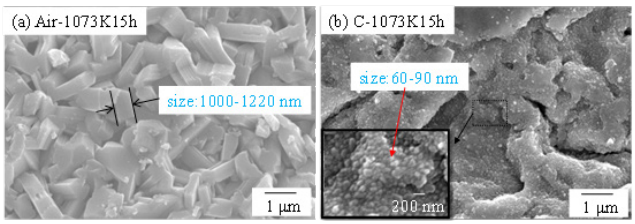



**Figure 23:** SEM images of surface morphology of the samples fabricated by (a) HT in the air and (b) cHT.

Bonding environment. Figure 24 shows the XPS results by investigating the samples of Air-1073K15h and C-1073K15h. For the O 1s high-resolution XPS spectra, the peak usual locates at 529.4 corresponds to the Ti-O banding for $TiO_2$ coatings. Figure 24a shows that the O 1s bonding energy of the C-1073K15h sample shows a shift to 529.8 eV, which could be related to the formation of oxygen vacancies [19, 65]. While figure 24b shows that the Ti 2p XPS spectra are almost identical, which hints that the Ti atoms is with a similar bonding environment after the HT in the air and cHT.

UV-vis spectroscopy was further used to study the electronic states of the samples of Air-1073K15h and C-1073K15h, as shown in figure 25. Compared with the absorbance of the Air-1073K15h sample, the absorbance edge of the C-1073K15h sample evidently moves towards the visible light region. Moreover, from figure 25a, the C-1073K15h sample shows strong absorption in almost the entire region.

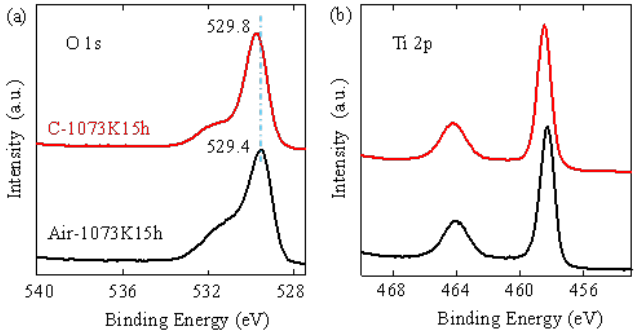



**Figure 24:** XPS spectra of the samples of Air-1073K15h and C-1073K15h. (a) O 1s XPS spectra, (b) Ti 2p XPS spectra. The labels in (a) applies to (b).

This change hints that the oxygen vacancies were formed in the lattice of $TiO_2$ during cHT. Figure 25b shows that the band gap narrows from 2.88 eV of the Air-1073K15h sample to 1.08 eV of the C-1073K15h sample. This result confirms that cHT could effectively narrow the band gap of the $TiO_2$, and hints that the formed oxygen vacancies in the lattice of $TiO_2$, which is consistent with the similar results reported by other researchers [19 , 67].

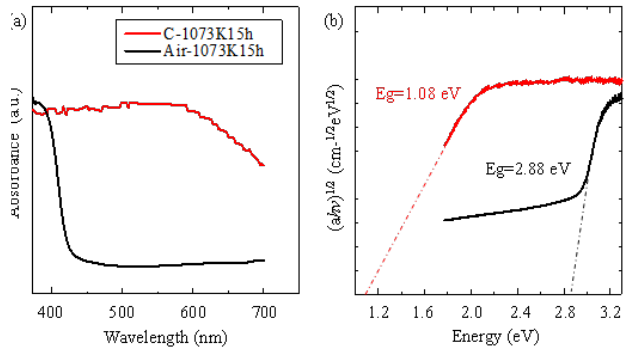



**Figure 25:** (a) UV-vis absorption spectra of the samples of Air-1073K15h and C-1073K15h; (b) Plots of (ahv)1/2 versus the photon energy (hv) of the UV-vis absorption spectra. The labels in (a) applies to (b).

Photocatalytic activity. The photocatalytic activity of the samples of Air-1073K15h and C-1073K15h was evaluated by degradation of MB solution under UV and visible light irradiation, as shown in figure 26. It could be found that the C-1073K15h sample shows a significant enhancement in the photocatalytic activity, compared with that of the Air-1073K15h sample. The enhancement of the photocatalytic activity of the C-1073K15h sample could be considered as the following reasons. The formed surface morphology with the nano-bump structure of the C-1073K15h sample substantially increases the accessible surface area. Moreover, the cHT is the main factor in narrowed band gap value from 2.88 eV to 1.08 eV, which could benefit the generation of electrons and holes to enhance the photocatalytic activity. In addition, the mixed crystal of TiCxOy and rutile $TiO_2$ of the C-1073K15h sample could increase the separation of charge transfer between TiCxOy and $TiO_2$.

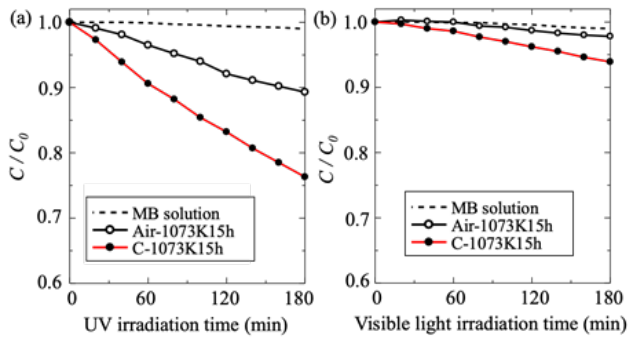



**Figure 26:** Comparison of the photocatalytic activity of the samples of Air-1073K15h and C-1073K15h. (a) Under UV irradiation, (b) Under visible light irradiation.

## Influence of cHT temperature on photocatalyst coatings

According to the successfully enhanced photocatalytic activity of C-doped $TiO_2$ coatings by cHT at 1073 K for 15h, the influence of cHT temperature and time were investigated. The Ti coatings were conducted by cHT at x (937, 1073, 1173, and 1273) K for y (2, 15, 30, and 50) h, using an electric furnace, and named as "C-xKyh".

Appearance. Figure 27 shows the appearance of the C-xK15h samples fabricated by cHT for Ti coatings. After cHT at different temperatures for 15 h, the C-xK15h samples appear various colors, with increasing the temperature from 973 to 1273 K. The color shows dark-blue at 973 K, brown at 1073 K, light-black at 1173 K and black at 1273 K.

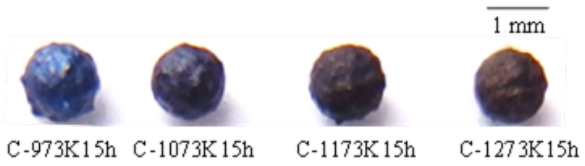



**Figure 27:** Appearance of the C-xK15h samples fabricated by cHT.

Formed compounds. Figure 28 shows XRD patterns of the C-xK15h samples. The influence of cHT temperature on the formed compounds of the Air-xK15h samples is obvious. After cHT at 1073 K, the C-1073K15h sample is with a mixed crystal of TiCxOy and rutile TiO2 forms on the surface of Ti coatings, as discussed above. When decreasing the cHT temperature to 973 K, the crystal shows slight TiCxOy and rutile $TiO_2$ (54.3°). While increasing the cHT temperature to 1173 K, the crystal becomes only TiCxOy, indicating that possibly formed $TiO_2$ had been reduced to be TiCxOy [68, 69]. The relative intensity of TiCxOy peak in the C-1173K15h sample is stronger than that of the C-1073K15h sample. When increasing the cHT temperature to 1273 K, the crystal shows that TiCxOy increases and Ti decreases, indicating that the formed amount of TiCxOy increased. The difference in color between the C-xK15h samples could be related to the crystal structure [19, 56].

Morphology evolution. Figure 29 shows that the change of the surface morphology of the C-xK15h sample fabricated by cHT under different HT temperatures for 15 h. In general,

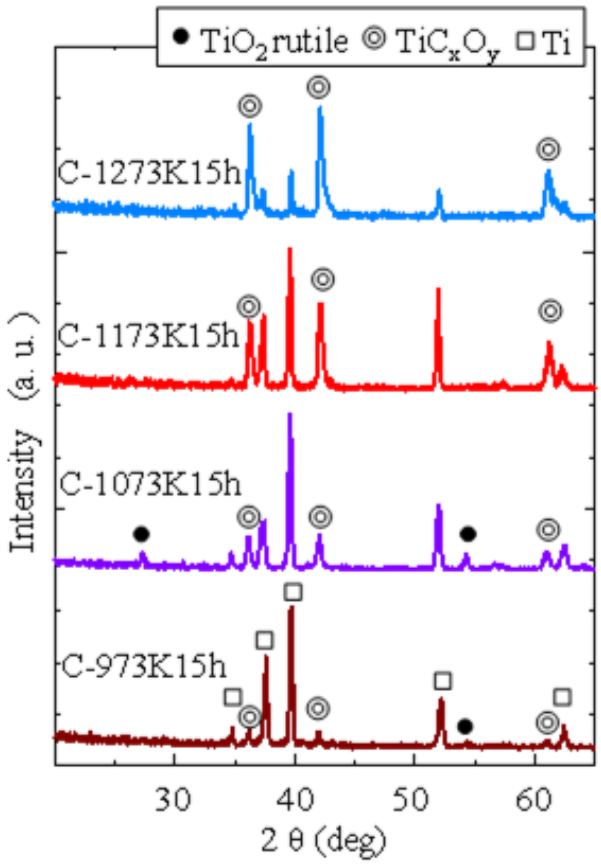



**Figure 28:** XRD patterns of the C-xK15h samples fabricated by cHT.

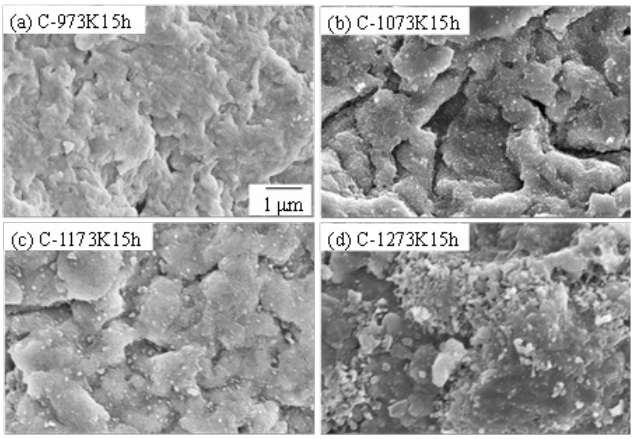



**Figure 29:** SEM images of surfaces of the C-xK15h samples fabricated by cHT. (a) C-973K15h, (b) C-1073K15h, (c) C-1173K15h, (d) C-1273K15h. The scale in all images is 1 μm.

it clearly shows the change of the size of formed compounds on the surface, with increasing cHT temperatures. When under relatively low cHT temperature of 973 K, the formed compound is difficult to be detected from the surface of the C-973K15h sample (Figure 29a), which hardly shows the change compared with that of Ti coatings. When increasing the cHT temperature to 1073 K, figure 29b shows that the formed compounds of the C-1073K15h sample are with the nano-bump structure. While increasing the cHT temperature to 1173 K, figure 29c also shows that the formed compounds of the C-1173K15h sample are with the nano-bump structure,

increasing in size and number. However, the formed compounds of the C-1273K15h sample become to micro structure, with increasing the cHT temperature to 1273 K. Hence, the remarkable change of the surface morphology could be related to the change of the crystal structure and the reaction process of Ti with the involved carbon oxide and its concentration, by cHT with different HT temperatures for 15 h.

Bonding environment. To further investigate the bonding environment of O, K, Ti and C elements in the samples, figure 30 shows the XPS results of the C-1073K15h and C-1173K15h samples. The peak of the O 1s high-resolution XPS spectra usually locates at 529.4, which could correspond to the Ti-O banding for $TiO_2$ coatings. It shows a significant shift of the O 1s peak to 529.9 eV of the C-1073K15h sample and 530.3 eV of the C-1173K15h sample, respectively. The shift of O 1s XPS spectra could be related to the formed oxygen vacancies in the crystal of $TiO_2$. Moreover, figure 30b clearly shows that the peak of Ti3+ forms in the Ti 2p XPS spectra, which further confirms the replacement of oxygen to form the oxygen vacancies. In addition, figure 30c shows that C 1s XPS spectra have been measured to investigate the carbon states in the photocatalyst. As we know, the peak nearby at 282.2 eV could be usually considered to the Ti-C bonds, which was observed from the C-1173K15h sample. This result hints that carbon may be doped into the crystal of $TiO_2$ under cHT [69, 70].

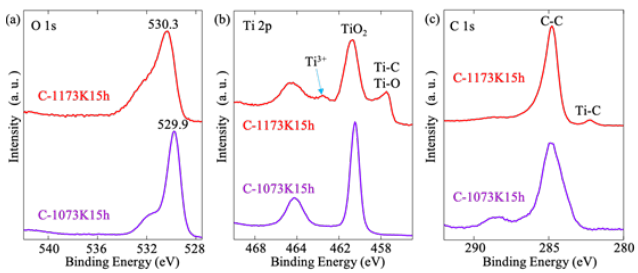



**Figure 30:** XPS spectra of the C-1073K15h and C-1173K15h samples. (a) O 1s XPS, (b) Ti 2p XPS, (c) C 1s XPS.

Photocatalytic activity. Figure 31 shows that the photocatalytic activity of the C-xK15h samples which is evaluated by degradation of MB solution under UV and visible light irradiation at room temperature. According to the concentration change of MB solution, the C-xK15h samples show photocatalytic activity. Compared with the influence of cHT temperature on photocatalytic activity under UV and visible light irradiation, the photocatalytic activity of the C-1173K15h sample is higher than those of the C-xK15h samples. While increasing the cHT temperature from 973 K to 1273 K, figure 31 shows the photocatalytic activity first increases and then decreases, which hints that photocatalytic activity is related to the crystal structure of $TiO_2$, the accessible surface area of the nano-bump structure, the doped carbon, and the formed oxygen vacancy in the crystal.

## Influence of cHT time on photocatalyst coatings

TBased on the above results of the C-xK15h samples, the influence of cHT time on photocatalyst coatings is focused on the HT temperature of 1073 K and 1173 K.

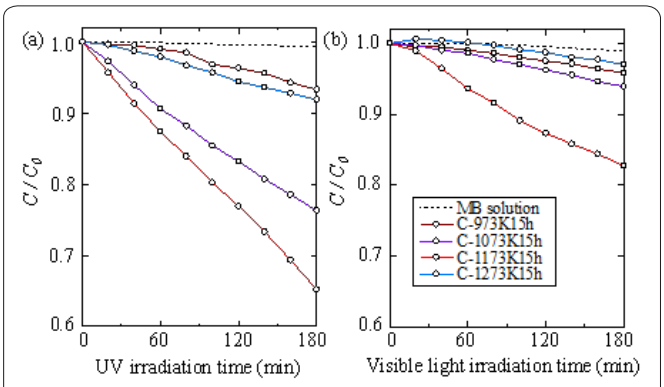



**Figure 31:** Photocatalytic activity comparison of the C-xK15h samples. (a) Under UV irradiation; (b) Under visible light irradiation. The labels in (b) applies to (a).

Appearance. After cHT with different temperatures and times, the C-xKyh samples appear in various colors, as shown in figure 32. With extending the cHT times at 1073 K, the color of the C-1073Kyh samples shows black and the color change to dark-brown (C-1073K50h) until extending the cHT time to 50 h. While extending the cHT times at 1173 K, the color of the C-1173Kyh samples changes from black (C-1173K15h) to light-black (C-1173K30h) and then brown (C-1173K50h).

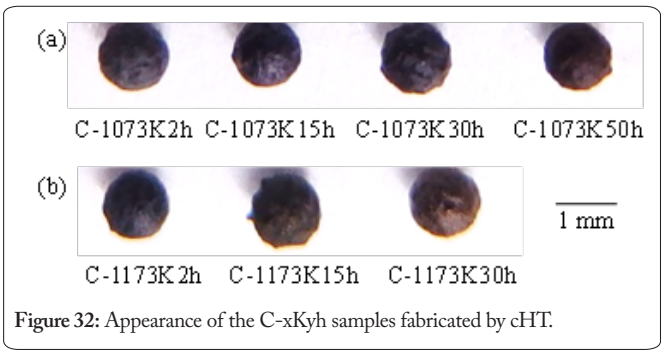



**Figure 32:** Appearance of the C-xKyh samples fabricated by cHT.

Formed compounds. Figure 33 shows XRD patterns of the C-xKyh samples. After cHT at 1073 K, figure 33a shows the influence of cHT time on the formed compounds of the C-1073Kyh samples are remarkable. The C-1073Kyh samples are with a mixed crystal of TiCxOy and rutile TiO2 forms

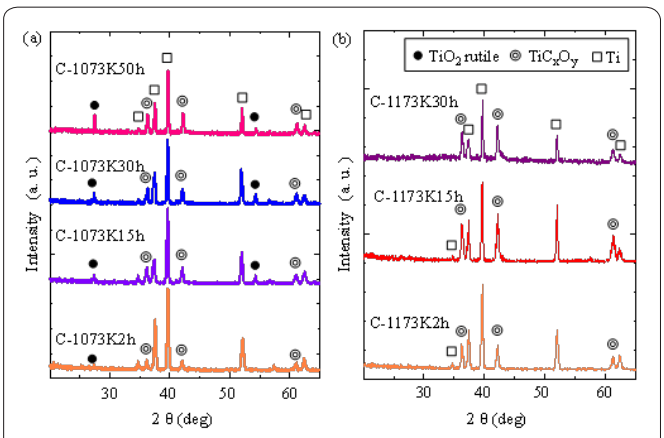



**Figure 33:** XRD patterns of the C-xK15h samples fabricated by cHT. The labels in (b) applies to (a).

on the surface of Ti coatings. With extending the cHT time from 2 h to 50 h at 1073 K, the relative intensity of rutile TiO2 peaks becomes stronger. After cHT at 1173 K, figure 33b shows the influence of cHT time on the formed compounds of the C-1073Kyh samples is slight. The C-1173Kyh samples are with only TiCxOy forms on the surface of Ti coatings. With extending the cHT time from 2 h to 30 h at 1173 K, the relative intensity of TiCxOy peaks first increases (C-1173K15h) then decreases (C-1173K30h). This change of the relative intensity of TiCxOy peaks may be related to the reduction of the possibly formed TiO2 [68, 69].

Morphology evolution. Figures 34 and 35 show that the influence of the cHT time at 1073 K and 1173 K on the surface morphology evolution using SEM, respectively. In general, with extending the cHT time from 2h to 50 h at 1073 K, the formed compounds with the nano-bump structure increase in number and grow in size. When the cHT time is short, the formed compound is difficult to be detected from the C-1073K2h sample (Figure 34a). When extending the cHT time to 15 h, from Figure 34b, the formed compounds grow in size and number which shows the nano-bump structure. Moreover, the surface morphology of the C-1073K30h sample is similar to that of the C-1073K15h sample. While extending the cHT time to 50 h, the reaction compounds significantly increase in size and the C-1073K50h sample shows a micro-bump structure (Figure 34d). Also, compared with the C-1073Kyh samples, figure 35 shows that the influence of the cHT time at 1173 K on the surface morphology of the C-1173Kyh samples, with increasing the cHT time at 1173 K. The formed compound is also difficult to be detected from the C-1173K2h sample, and the formed compounds increase in size and the C-1173K15h sample shows the nano-bump structure. While extending the cHT time to 30 h, the formed compounds obviously increase and the C-1173K30h sample shows micro structure.

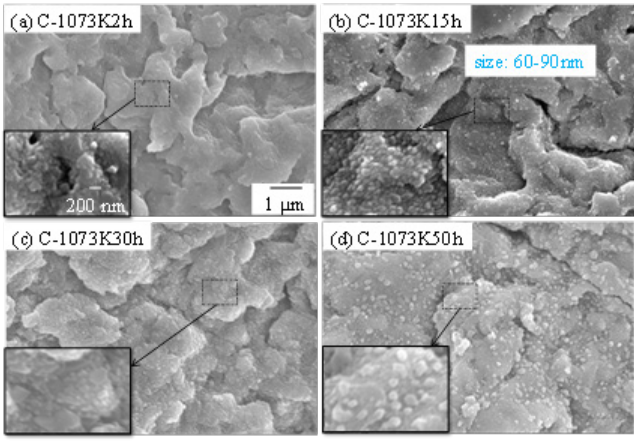



**Figure 34:** SEM images of surfaces of the C-1073Kyh samples fabricated by cHT. (a) C-1073K2h, (b) C-1073K15h, (c) C-1073K30h, (d) C-1073K50h. The scale in all images is 1 μm.

Photocatalytic activity. Figure 36 shows the degradation rate constant of the photocatalytic activity of the C-1073Kyh samples by degradation of MB solution under UV and visible light irradiation. The trend of photocatalytic activity

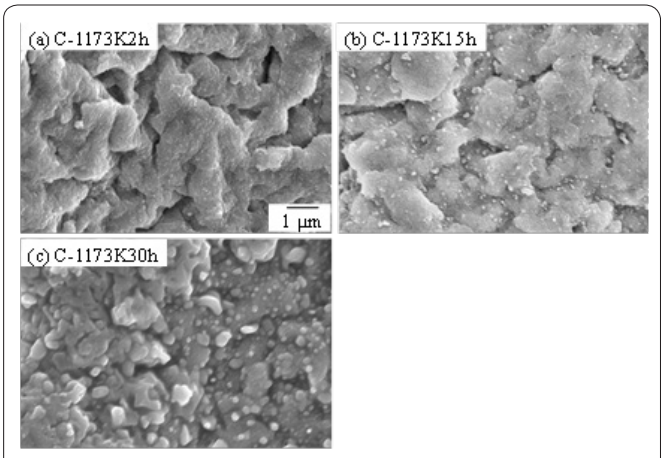



**Figure 35:** SEM images of surfaces of the C-1173Kyh samples fabricated by cHT. (a) C-1173K2h, (b) C-1173K15h, (c) C-1173K30h. The scale in all images is 1 μm.

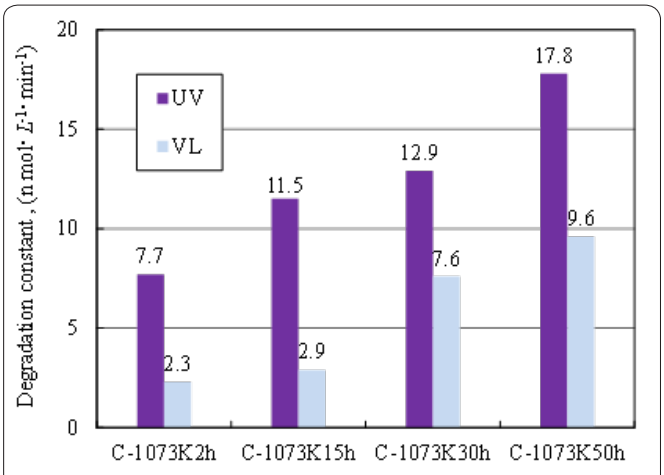



**Figure 36:** Degradation constant rate of the photocatalytic activity of the C-1073Kyh samples.

of the C-1073Kyh samples increases, with increasing the cHT times. The enhancement of photocatalytic activity of the C-1073K15yh samples may be considered to the formed nano-bump morphology and mixed crystal of TiCxOy and rutile $TiO_2$. The formed nano-bump morphology significantly increases the accessible surface area. In addition, the mixed crystal of TiCxOy and rutile $TiO_2$ could increase the separation of charge transfer between TiCxOy and $TiO_2$. While the trend of photocatalytic activity of the C-1173Kyh samples first increases and then decreases with increasing the cHT times, as shown in figure 37. The reason for photocatalytic activity of the C-1173K15yh samples may be attributed to the change of surface morphology, the relative intensity of TiCxOy.

## Modification strategy of the effect of charge transfer

To overcome the limitation of single-component photocatalysts, it is possible to construct the photocatalysis systems by suppressing the recombination of the electron-hole pairs through charge transfer. Recently, heterojunctions formed between two solid materials have attracted more and more attention, which could include the heterojunctions

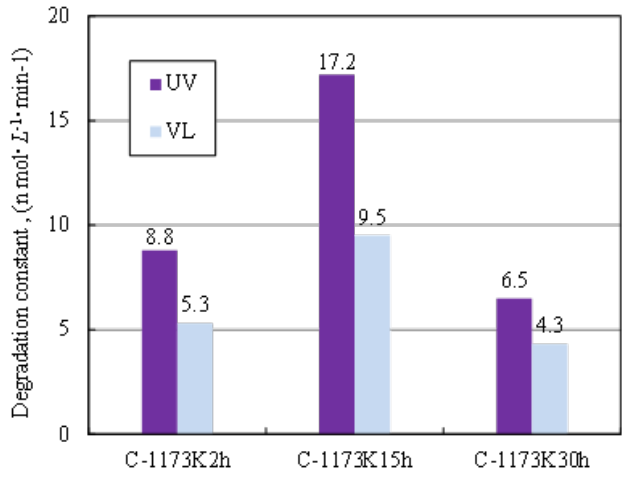



**Figure 37:** Degradation constant rate of the photocatalytic activity of the C-1173Kyh samples.

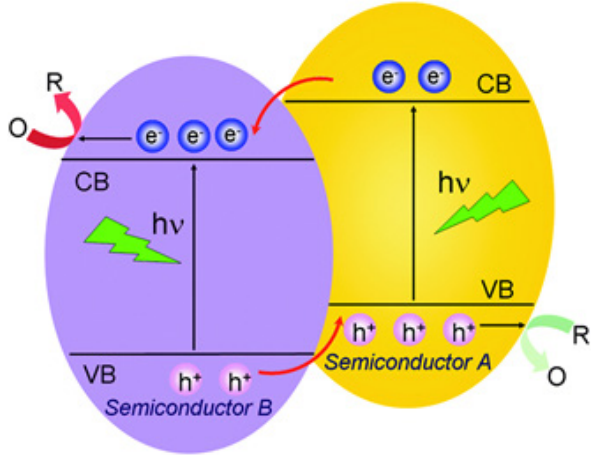



**Figure 38:** Heterojunction photocatalysts and the effect of charge transfer.

between semiconductor/semiconductor, semiconductor/metal, and semiconductor/carbon (carbon nanotubes, graphene, etc.). Till the current date, the most developed heterojunction is based on a semiconductor/semiconductor, usually between a semiconductor and $TiO_2$ in close contact. The photo-generated charge transfer of electrons and holes at the interface of semiconductor/$TiO_2$ has been intensively studied because understanding the interfacial charge transfer is crucial to the development of numerous devices [22, 72]. A large amount of research work has been devoted to the study of charge transfer, separation, and recombination phenomena. Coupling between different semiconductors in photocatalytic systems was used to form the heterojunction structure to enhance the charge transfer. But the coupled semiconductors do not always increase the charge transfer, because the coupled semiconductor relies on the band structures of each component, which is also affected by many other factors, such as surface area, defect density, crystallinity, and quantum size effects. Hereafter, the main visible light-responsive heterojunction photocatalysts of semiconductor/$TiO_2$ have been summarized as follows, and they have the greatest potential to be used for large-scale applications.

Therefore, this part will focus on the enhancement of the photocatalytic activity of photocatalyst coatings by the effect of charge transfer via heterojunction, as shown in figure 38 [73], such as the TiC/$TiO_2$ and GO/$TiO_2$ composite photocatalyst coatings.

## TiC/$TiO_2$ composite photocatalyst coatings

In this part, we proposed an approach to enhance the photocatalytic activity of $TiO_2$ photocatalyst coatings by the effect of charge transfer between $TiO_2$ and TiC, via a simple method of changing the Ti coatings to TiC coatings. Firstly, TiC coatings were coated on $Al_2O_3$ balls by mechanical coating operation with TiC powder (purity of 99%, diameter: 2-5 μm, Kojundo Chemical), and named as "TiC". Then TiC coatings were annealed in carbon powder and in the air at 1073 K for 15 h and named "TiC-C-1073K15h" and "TiC-Air-1073K15h", respectively.

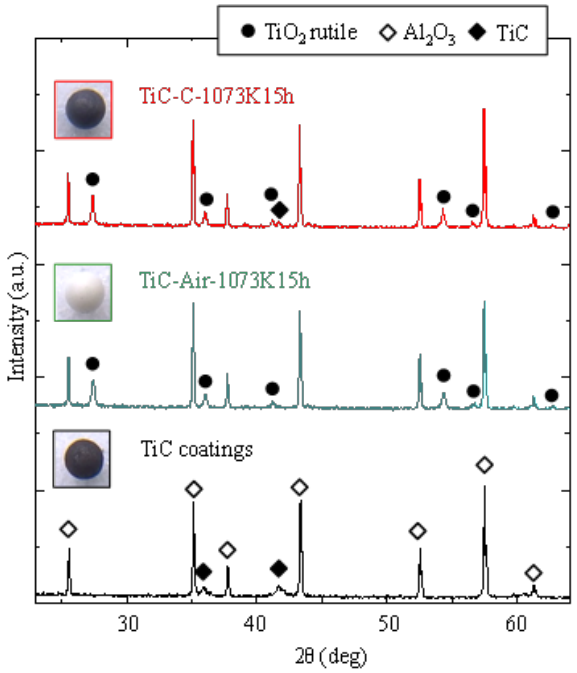



**Figure 39:** Appearance and XRD patterns of the samples of TiC-C-1073K15h and TiC-Air-1073K15h

Appearance and formed compounds. Figure 39 shows the appearance and XRD patterns of the samples of TiC-C-1073K15h and TiC-Air-1073K15h. The TiC-C-1073K15h sample consists of a mixture of rutile $TiO_2$ and TiC, appearing black. While the TiC-Air-1073K15h sample is only rutile $TiO_2$ but shows white. This difference may be related to the reaction process. During HT in carbon powder, TiC and oxocarbon (COx) presumably react to form rutile TiO2 on the outside of TiC, resulting in heterojunctions of $TiO_2$/TiC, similarly to the previous report of controlled oxidation of TiC [63, 74, 77]. A possible reaction for the surface of TiC with oxocarbon is proposed in equation (3). During HT in the air, TiC directly reacts with oxygen, resulting in the oxidation of TiC to TiO2 with sufficient oxygen. The possible reaction for TiC in the air is proposed in equation (4).

$$TiC + COx \leftrightharpoons TiO_2 + C \quad (3)$$

$$TiC + O2 \leftrightharpoons TiO_2 + CO_2 \quad (4)$$

Morphology evolution. The surface morphology of the samples of TiC-C-1073K15h and TiC-Air-1073K15h are presented in Figure 40. The TiC-C-1073K15h sample shows a granular surface with a porous-like structure (Figure 40a), which is different from that of TiC (Figure 41a). It hints that rutile $TiO_2$ formed on the surface of TiC during HT in carbon powder. Moreover, the size of the surface morphology significantly increases, with extending the HT time in carbon powder from 2 h to 15 h at 1073 K (Figures 41b-d). On the other hand, the surface morphology of the TiC-Air-1073K15h sample shows a micro-bump structure (Figure 40b). It is known that the growth of $TiO_2$ during the HT process is dependent on the predominant diffusion of TiC and oxocarbon, which is influenced by the HT conditions and the concentration of oxocarbon [76-79]. Hence, the differences in surface morphology can be attributed to the different $TiO_2$ growth rate and the adsorption/desorption behavior of oxocarbon/oxygen on $TiO_2$ crystal structure.

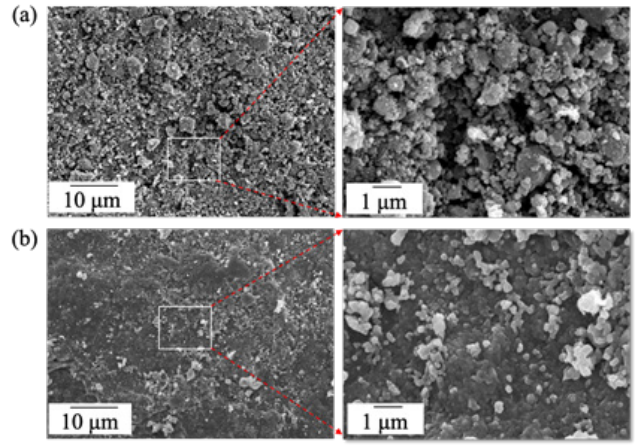



**Figure 40:** SEM images of surfaces of the samples of TiC-C-1073K15h and TiC-Air-1073K15h.

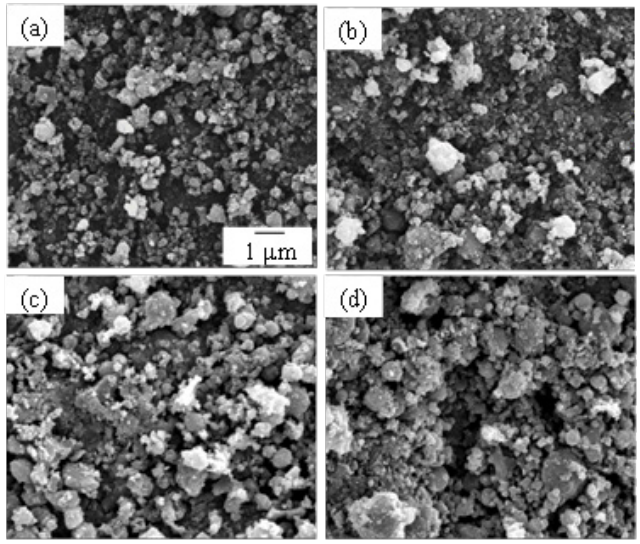



**Figure 41:** SEM images of surfaces of the samples fabricated by different cHT times. (a) TiC coatings, (b) TiC-C-1073K2h, (c) TiC-C-1073K5h, (d) TiC-C-1073K15h. The scale in all images is 1 μm.

Bonding environment. The UV-vis absorption spectra are used to investigate the electronic states of the samples of TiC-C-1073K15h and TiC-Air-1073K15h, as shown in figure 42. The TiC-Air-1073K15h sample shows the typical absorbance of pristine $TiO_2$. Whereas in the TiC-C-1073K15h sample, the absorbance edge evidently moves towards the visible-light range, showing strong absorption in almost entire region. It could be attributed to the generation of oxygen vacancies on the surface of the rutile $TiO_2$ [78-81].

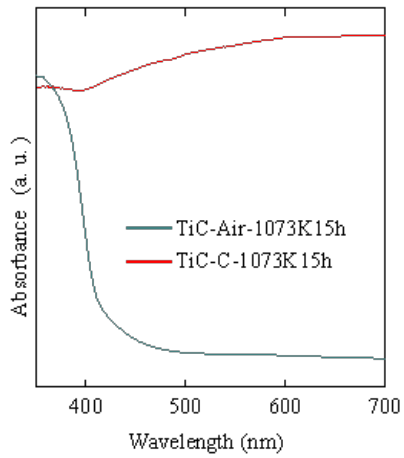



**Figure 42:** UV-vis absorption spectra the samples of TiC-C-1073K15h and TiC-Air-1073K15h.

Moreover, the PL emission spectra can be used to reveal the efficiency of the trapping and transfer of the pairs of electron and hole, and to understand the fate of the recombination of electron and hole [82-84]. Figure 43 shows the peak position of PL emission band of the TiC-Air-1073K15h sample is about 580 nm in the wavelength range of 530-660 nm. While the PL intensity of the TiC-C-1073K15h sample greatly decreased. The variation of PL intensity may result from the change of defect state of oxygen vacancies on the shallow level of the $TiO_2$ surface [83, 84], and the decrease in recombination rate between the photo-generated charge carriers [85, 86].

To further verify the formation of the active species in enhancement of photocatalytic activity, the 5,5-dimethyl-1-pyrroline-N-oxide (DMPO) spin-trapping EPR spectra was performed to characterize the photo-generated reactive

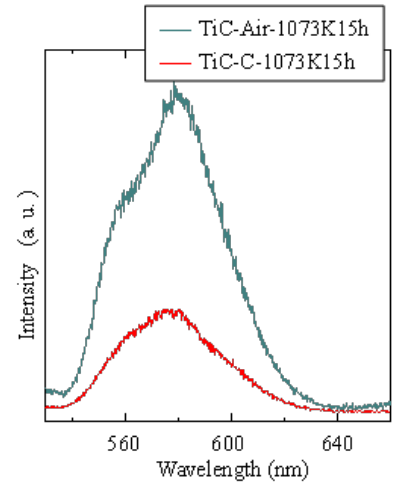



**Figure 43:** PL spectra of the samples of TiC-C-1073K15h and TiC-Air-1073K15h

oxygen species, under UV irradiation for 10 min. The characteristic four peaks of DMPO-OH• with intensity 1:2:2:1 can be clearly observed in the ESR signal (Figure 44), and this is similar to the spectra reported by other researchers [87-89]. It elucidates that OH• radicals are generated under UV irradiation, and no signals are observed under dark conditions. The intensity of EPR signal of the DMPO-OH• adduct was remarkably enhanced in the presence of the TiC-C-1073K15h sample under UV irradiation, as compared with that of the TiC-Air-1073K15h sample.

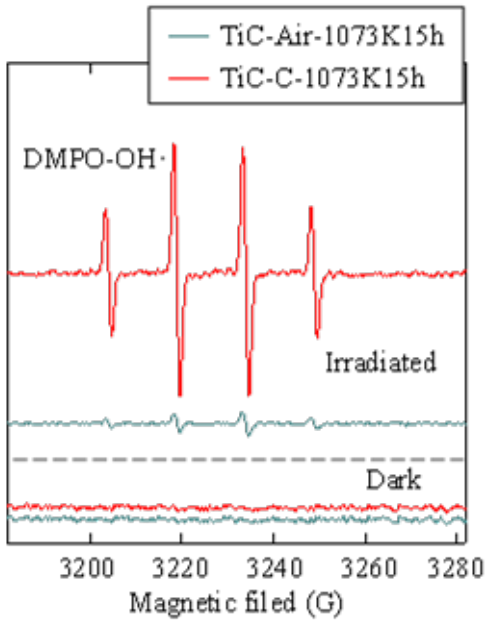



**Figure 44:** DMPO spin-trapping EPR spectra of the samples of TiC-C-1073K15h and TiC-Air-1073K15h.

Furthermore, we also examined the change of the surface chemical bonding of the TiC-C-1073K15h and TiC-Air-1073K15h samples with XPS spectra. The XPS survey spectra of the samples confirm the existence of Ti, O and C elements (Figure 45a). The O 1s XPS spectra of the samples of TiC-C-1073K15h and TiC-Air-1073K15h show dramatic differences (Figure 45b). The single O 1s peak at 529.4 eV in the TiC-Air-1073K15h sample (white $TiO_2$) comes from Ti-O-Ti linkages in $TiO_2$, whereas in the TiC-C-1073K15h sample (black $TiO_2$/TiC), this peak shows a significant shift to 530.3 eV. This shift of O 1s peak could be considered to the formation of the oxygen vacancies [89], which could increase the visible-light absorption and enhance the photocatalytic activity [90, 91]. However, Figure 45c shows that the Ti 2p peaks are almost identical for the black and white TiO2, indicating that the Ti atoms are with a similar bonding environment [90]. Also, the results of the C 1s XPS spectra (Figure 45d) reveal that the two samples are not doped with carbon or residual carbon [36].

Photocatalytic activity. Before the photocatalytic tests, a dark absorption (C: 20 μmol/L) of all samples was conducted for 18 h to reach complete adsorption-desorption equilibrium. We find that cHT for TiC coatings could exhibit a remarkable enhancement on the photocatalytic degradation of MB

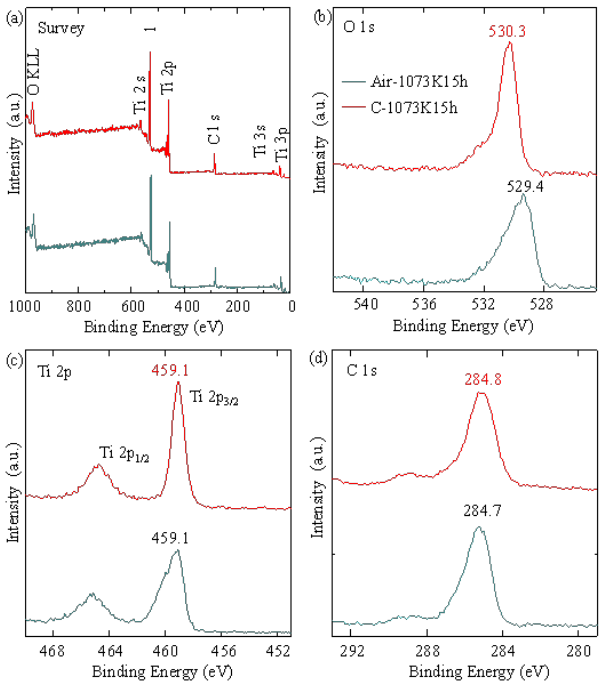



**Figure 45:** XPS spectra of the samples of TiC-C-1073K15h and TiC-Air-1073K15h. (a) Survey. (b) O 1s. (c) Ti 2p. (d) C 1s. The label in (b) applies to (a-d).

solution (C0: 10 μmol/L) under both visible light and UV irradiation (Figure 46). In particular, the visible-light photocatalytic activity was found to be fundamentally enhanced (Figure 46a), with a degradation rate more than 30 times higher than that of the TiC-Air-1073K15h sample. Moreover, the enhancement of photocatalytic activity due to heat treatment in carbon powder for TiC coatings is higher than that for Ti coatings (Figure 47). The results of cycle tests for the TiC-

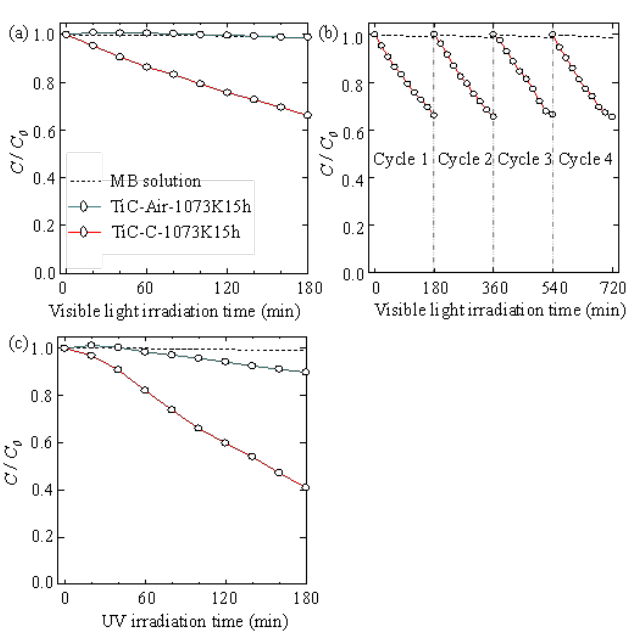



**Figure 46:** Comparative photocatalytic degradation of MB solution of the samples of TiC-C-1073K15h and TiC-Air-1073K15h. (a) Under visible light irradiation, (b) Cycle tests for the TiC-C-1073K sample under visible light irradiation. (c) Under UV irradiation. The label in (a) applies to (a-c).

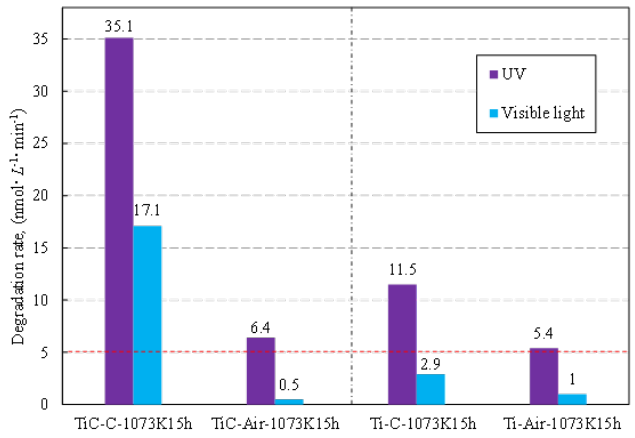



**Figure 47:** Photocatalytic degradation rate of MB solution by the samples under visible light and UV irradiation. The standard degradation rate for determining the performance of 5 nmol L-1 min-1 (red dashed line), obtained from the Photocatalysis Industry Association of Japan. (http://www.piaj.gr.jp/roller/en/entry/20090121)

C-1073K15h sample are shown in figure 46b. No apparent deactivation could be found after four runs, revealing that the TiC-C-1073K15h sample possesses excellent photocatalytic stability. Based on these results, we further investigate HT times in carbon powder for TiC coatings. The photocatalytic activity under visible light and UV irradiation slightly decreases with extending HT times at 1073 K (Figure 48).

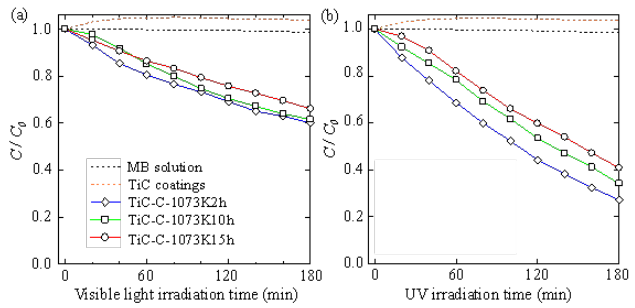



**Figure 48:** Comparative photocatalytic degradation of MB solution by the samples fabricated under 1073 K for different holding times. (a) Under visible light. (b) Under UV irradiation. The label in (a) applies to (b).

The increasing visible-light absorption and enhancing photocatalytic activity of the black $TiO_2$/TiC coatings could be attributed to the following three reasons. The granular surface with the porous-like structure of black $TiO_2$/TiC coatings increases the accessible surface area. Another is the heterojunctions of $TiO_2$/TiC, which could promote the charge transfer of the photogenerated electron-hole pairs [92]. It also has been confirmed by the decreased PL intensity and the increased intensity of DMPO spin-trapping EPR spectra. More importantly, oxygen vacancies generated in the lattice of $TiO_2$ act as electron traps, and the proposed bandgap structure model is shown in figure 49. Moreover, the generated oxygen vacancies are confirmed by the dramatic shift of the O 1s XPS spectra. Accordingly, the increased visible light absorption benefits the generation of more photogenerated electron-hole pairs, and the heterojunctions of $TiO_2$/TiC promote the separation by the charge transfer to further enhance the photocatalytic activity. To the best of our knowledge, our

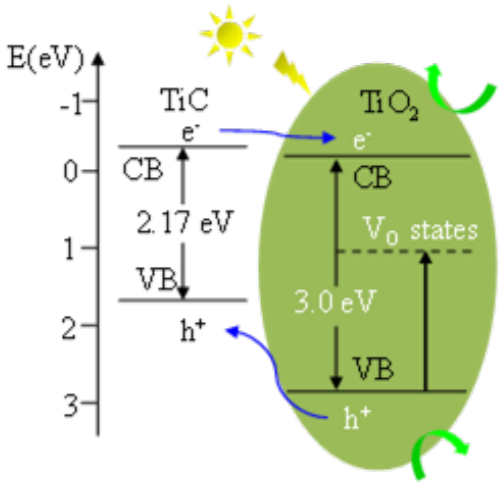



**Figure 49:** Schematic illustration of proposed bandgap structure model for the charge transfer. VO state is due to the generated oxygen vacancies, VB and CB represent the valence band and the conduction band, respectively.

finding constitutes the first experimental evidence of the visible light photocatalytic activity of black $TiO_2$/TiC coatings fabricated by HT in carbon powder for TiC coatings, which were prepared by MCT with TiC powder on $Al_2O_3$ balls, using a safe, low-cost, and effective approach.

## GO/$TiO_2$ composite photocatalyst coatings

In this part, we also tried another approach to enhance the photocatalytic activity of $TiO_2$ photocatalyst coatings by the effect of charge transfer between $TiO_2$ and GO, via a simple method of electrophoretic deposition (EPD) to attach GO onto the surface of $TiO_2$ coatings. Firstly, $TiO_2$ coatings were prepared using Ti powder by mechanical coating operation and followed multi-heat treatment (pretreatment in carbon powder-oxidation in air-reduction in carbon powder), and the coatings were denoted as "Ti-mHT". The detailed multi-heat treatment process was described in the supplemental materials [71]. Then GO has been combined with the prepared TiO2 coatings by EPD. The TiO2 coatings are tiled on a steel plate, and soaked in GO dispersion solution (100ml, 1 mg/L), as shown in Figure 50a. The distance of the positive and negative steel plates is 1.5 cm. The EPD is carried out at 25 °C under a power supply of 10 V, with extending its time and named as "GO1-10Vxh", with GO1 being the concentration of GO solution and x being the EPD time.

Formed compounds. XRD patterns and Raman spectroscopy of the samples are presented in Figure 50b and 50c. The diffraction peaks of the formed TiO2 rutile are significant, after mHT for Ti coatings. While any change could be found from the Ti-mHT and GO1-10V3h samples (Figure 51). From Figure 50c, the D and G peaks around 1345 and 1600 cm-1 observed from the Ti-mHT sample verifies the influence of the amorphous carbon formed on the surface during mHT or the graphitization of carbon present in TiO2 [71, 93]. While the increased intensity of the D and G peaks indicates that the combined GO on the surface of TiO2 coatings, even with only 1 min. With extending the EPD time, the relative intensity of the G peak becomes improved, indicating

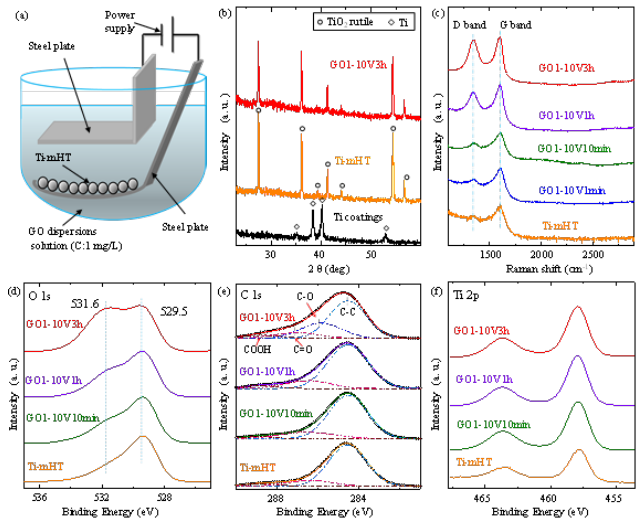



**Figure 50:** Characterization of the samples. (a) Scheme of the electrophoresis deposition, (b) XRD patterns, (c) Raman spectra, (d-f) XPS spectra.

the increased amount of combined GO. Meanwhile, the peak around 529.5 eV from the O 1s spectra of the samples (Figure 50d), is generally known to the O2- ions, surrounded by the Ti ions [88], while the peak around 531.6 eV could be attributed to the formed hydroxyl groups from GO [93]. Notably, along with the extended EPD time, the relative intensity of the hydroxyl groups becomes improved, which could significantly enhance the light absorption [93, 94]. Furthermore, Figure 50e shows that the GO1-10V3h sample exhibits the typical peaks at 284.5, 285.9, 287.3, and 288.9 eV resulting from C-C, C-O, C=O, and HO-C=O groups, respectively [94, 95]. With extending the EPD time, the oxygen-containing functional groups become improved, especially the C-O group from that of the GO1-10V3h sample. It means that the amount of GO on the surface of TiO2 coatings could be increased, by extending the EPD time. Moreover, the change of Ti 2p spectra is insignificant (Figure 50f), indicating a similar bonding environment for Ti atom.

Surface morphology evolution. The surface morphology of the sample analyzed using SEM is presented in Figure 52. By contrast with that of the Ti-mHT sample, the change in the combination of GO is significant with extending EPD time, starting from 10 min. When the EPD time is more than 1 h, the formed GO becomes more evident, with increasing in

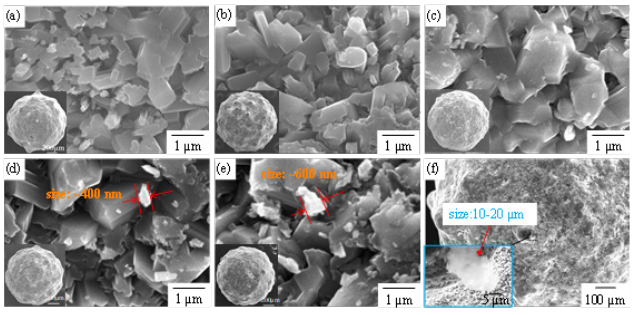



**Figure 52:** Surface morphology evolution of the samples. (a) Ti-mHT, (b) GO1-10V1min, (c) GO1-10V10min, (d) GO1-10V1h, and (e-f) GO1-10V3h.

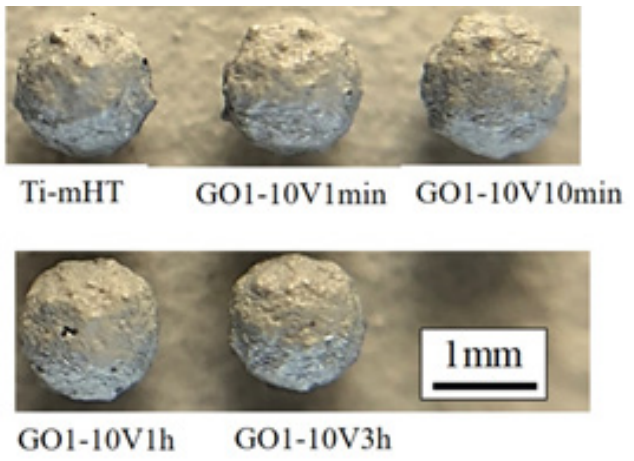



**Figure 51:** Appearance of the samples.

number and size. In the case of the GO1-10V3h sample, Figure 52e indicates that the size of GO is around 100-600 nm, while some larger powder-like GO could be observed, with the size of 10-20 μm (Figure 52f). It means that a relatively large amount of GO has been successfully formed on the surface of TiO2 coatings, which could substantially enhance the light absorption and increase the accessible surface area of the photocatalyst coatings [91, 94].

Photocatalytic activity and stability. Figure 53 reveals that the GO1-10Vx samples exhibit excellent photocatalytic activity and stability. In general, with extending the EPD time, Figure 53a-b clearly shows that the photocatalytic activity of the GO1-10Vxh samples continuously enhances, with an increased rate constant by approximately one to two times (Table. 2). Compared with that of only mechanical-stirring without EPD (Figure 54), the GO1-10Vx samples perform a higher photocatalytic activity, which could substantially shorten treatment time. While Figure 53c-d reveals that the TiO2 coatings combined with GO could effectively enhance the photocatalytic activity under visible light. It could conclude that the photocatalytic activity is directly related to the formed GO on the surface of TiO2 coatings, with the hydroxyl groups and nano-size structure [94,95].

**Table 2:** Comparison of pseudo-first-order model parameters, rate constants (k, min-1) and R2 towards the degradation of MB solution. VL is visible light.

| Sample | $k$ (min$^{-1}$) | $R^2$ |
|---|---|---|
| Ti-mHT UV | 0.0013 | 0.997 |
| GO1-10V1min UV | 0.0017 | 0.997 |
| GO1-10V10min UV | 0.0017 | 0.993 |
| GO1-10V1h UV | 0.0024 | 0.992 |
| GO1-10V3h UV | 0.0028 | 0.995 |
| Ti-mHT VL | 0.0005 | 0.961 |
| GO1-10V3h VL | 0.0011 | 0.973 |

To further confirm the photocatalytic stability, eleven cycle tests were conducted for the GO1-10V3h sample (Figure 53e). The concentration of MB solution for multiple tests continues to decrease to more than 70%, indicating a satisfactory stability. Furthermore, the influence the combination of TiO2

and GO of the coatings on the photocatalytic stability is evaluated. Even after an ultrasonic cleaning, Figure 53f shows that the photocatalytic activity of the GO1-10V3h sample tends to be stable. The schematic diagram of the charger transfer between TiO2 and GO is proposed and presented in Figure 53g. Therefore, the significant enhanced photocatalytic activity and stability could be attributed to the formed GO, with the formed hydroxyl groups and larger accessible surface area, as well as the effect of charge transfer.

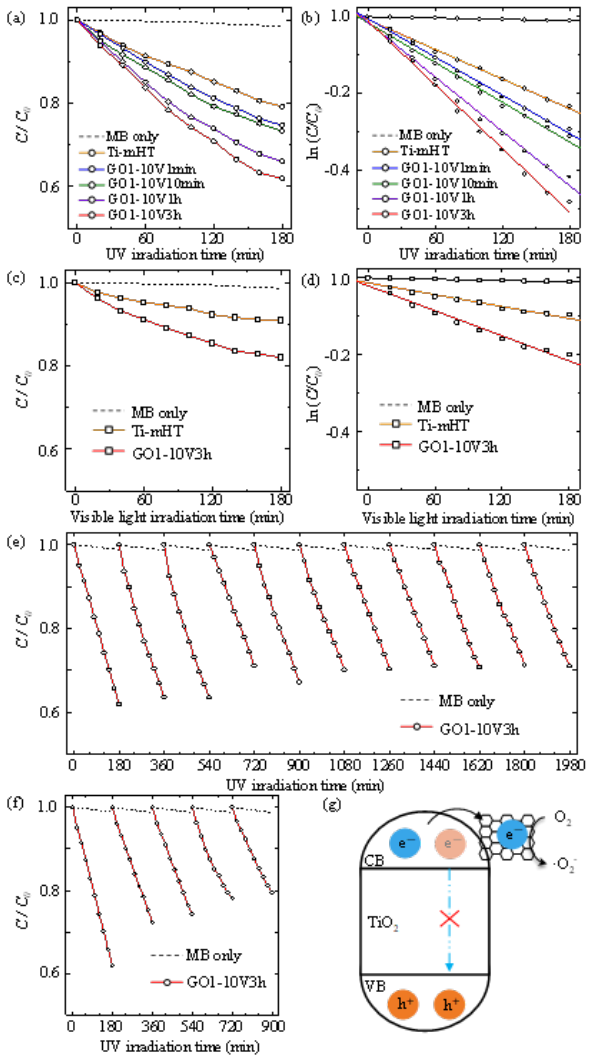



**Figure 53:** Comparison of photocatalytic activity and stability towards degradation of MB solution. (a-b) Under UV, (c-d) Under visible light, (e) Cycle tests, (f) Cycle tests after ultrasonic cleaning with every 10 min, (g) Schematic illustration of charge transfer.

It can be concluded that the TiO2/GO composites coatings exhibit a substantially enhanced photocatalytic activity and stability, owing to the formed GO with hydroxyl groups and larger accessible surface area, as well as the effect of charge transfer between TiO2 and GO.

## Summary and prospect

This review presents the latest results of studies directed at modification strategies on the TiO2 photocatalyst coatings.

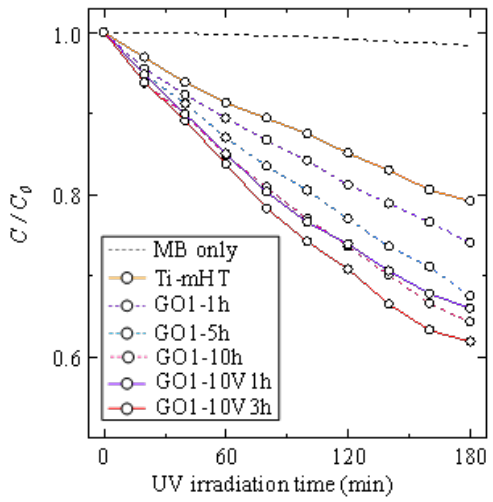



**Figure 54:** Comparison of the photocatalytic activity towards the degradation of MB solution for the GO1-10Vxh and GO1-xh samples. The GO1-10Vxh samples are prepared by EPD. The GO1-1xh samples are prepared by only mechanical-stirring without EPD.

The modification strategies encompass porous structure, nano-surface, carbon-doping, combination with TiC and graphene oxide. According to these modification strategies, the approaches encompass sulfuric-acid-bath treatment (SAT), carbon-embedding heat treatment (cHT), heterojunction photocatalysts of TiC/TiO2 and electrophoretic deposition (EPD). Compared with the enhancement of photocatalytic activity of TiO2 coatings, these approaches all show their different characteristics and advantages. SAT could effectively generate the porous structure on Ti coatings, cHT significantly increase the visible-light response and enhances the photocatalytic activity, and EPD shows a simple way to further enhance the photocatalytic activity via the effect of charge transfer between the combined GO and TiO2.

Notably, according to the characteristics and advantages of the above modification strategies, this review also proposes a synergistic strategy of the combination of SAT, cHT and EPD to further enhance the photocatalytic activity of TiO2 coatings, as shown in Figure 55. Compared with traditional

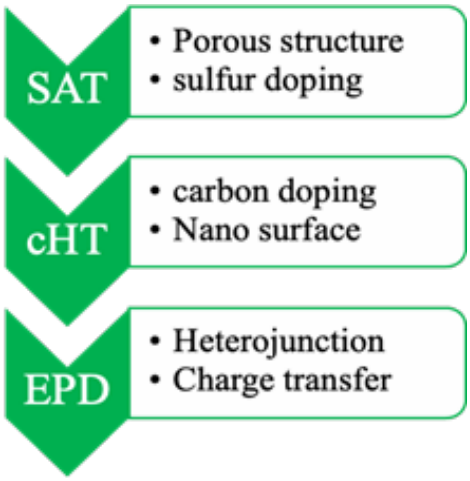



**Figure 55:** Synergistic strategy of SAT, cHT and EPD to prepare high-performance photocatalyst materials.

coating techniques, this synergistic strategy is expected to become an effective method to fabricate the next-generation photocatalyst matericals, with satisficant photocatalytic activity to meet the application.

## References


1. Yang H, Xu Z, Fan M, Gupta R, Slimane RB, et al. 2008. Progress in carbon dioxide separation and capture: a review. *J Environ Sci (China)* 20(1): 14-27. https://doi.org/10.1016/s1001-0742(08)60002-9
2. Dincer I, Rosen MA. 1998. A worldwide perspective on energy, environment and sustainable development. *Int J Energy Res* 22(15): 1305-1321. https://doi.org/10.1002/(SICI)1099-114X(199812)22:15%3C1305::AID-ER417%3E3.0.CO;2-H
3. Panwar NL, Kaushik SC, Kothari S. 2011. Role of renewable energy sources in environmental protection: A review. *Renew Sustain Energy Rev* 15(3): 1513-1524. https://doi.org/10.1016/j.rser.2010.11.037
4. Fujishima A, Honda K. 1972. Electrochemical photolysis of water at a semiconductor electrode. *Nature* 238(5358): 37-38. https://doi.org/10.1038/238037a0
5. Thompson TL, Yates JT. 2006. Surface science studies of the photoactivation of TiO2--new photochemical processes. *Chem Rev* 106(10): 4428-4453. https://doi.org/10.1021/cr050172k
6. Mor GK, Varghese OK, Paulose M, Shankar K, Grimes CA. 2006. A review on highly ordered, vertically oriented TiO2 nanotube arrays: Fabrication, material properties, and solar energy applications. *Sol Energy Mater Sol Cells* 90(14): 2011-2075. https://doi.org/10.1016/j.solmat.2006.04.007
7. Ni M, Leung MKH, Leung DYC, Sumathy K. 2007. A review and recent developments in photocatalytic water-splitting using TiO2 for hydrogen production. *Renew Sustain Energy Rev* 11(3): 401-425. https://doi.org/10.1016/j.rser.2005.01.009
8. Fujishima A, Zhang X, Tryk D. 2008. TiO2 photocatalysis and related surface phenomena. *Surf Sci Rep* 63(12): 515-582. https://doi.org/10.1016/j.surfrep.2008.10.001
9. Hoffmann MR, Martin ST, Choi WY, Bahnemann DW. 1995. Environmental applications of semiconductor photocatalysis. *Chem Rev* 95(1): 69-96. https://doi.org/10.1021/cr00033a004
10. Kumar SG, Devi LG. 2011. Review on modified TiO2 photocatalysis under UV/visible light: Selected results and related mechanisms on interfacial charge carrier transfer dynamics. *J Phys Chem A* 115(46): 13211-13241. https://doi.org/10.1021/jp204364a
11. Dozzi MV, Selli E. 2013. Doping TiO2 with p-block elements: Effects on photocatalytic activity. *J Photochem Photobiol C Photochem Rev* 14: 13-28. https://doi.org/10.1016/j.jphotochemrev.2012.09.002
12. Qian R, Zong H, Schneider J, Zhou G, Zhao T, et al. 2019. Charge carrier trapping, recombination and transfer during TiO2 photocatalysis: An overview. *Catal Today* 335: 78-90. https://doi.org/10.1016/j.cattod.2018.10.053
13. Linsebigler AL, Lu G, Yates JT. 1995. Photocatalysis on TiO2 surfaces: principles, mechanisms, and selected results. *Chem Rev* 95(3): 735-758. https://doi.org/10.1021/cr00035a013
14. Bouras P, Stathatos E, Lianos P. 2007. Pure versus metal-ion-doped nanocrystalline titania for photocatalysis. *Appl Catal B* 73(1-2): 51-59. https://doi.org/10.1016/j.apcatb.2006.06.007
15. Barnard AS, Xu H. 2008. An environmentally sensitive phase map of titania nanocrystals. *ACS Nano* 2(11): 2237-2242. https://doi.org/10.1021/nn800446w
16. Gu DE, Lu Y, Yang B, Hu Y. 2008. Facile preparation of micro-mesoporous carbon-doped TiO2 photocatalysts with anatase crystalline walls under template-free condition. *Chem Commun (Camb)* (21): 2453-2455. https://doi.org/10.1039/b800596f
17. Asahi R, Morikawa T, Ohwaki T, Aoki K, Taga Y. 2001. Visible-light photocatalysis in nitrogen-doped titanium oxides. *Science* 293(5528): 269-271. https://doi.org/10.1126/science.1061051
18. Valentin CD, Pacchioni G, Selloni A. 2005. Theory of carbon doping of titanium dioxide. *Chem Mater* 17(26): 6656-6665. https://doi.org/10.1021/cm051921h
19. Chen X, Liu L, Yu P, Mao SS. 2011. Increasing solar absorption for photocatalysis with black hydrogenated titanium dioxide nanocrystals. *Science* 331(6018): 746-750. https://doi.org/10.1126/science.1200448
20. Diebold U, Ruzycki N, Herman GS, Selloni A. 2003. One step towards bridging the materials gap: surface studies of TiO2 anatase. *Catal Today* 85(2-4): 93-100. https://doi.org/10.1016/S0920-5861(03)00378-X
21. Ren W, Ai Z, Jia F, Zhang L, Fan X, et al. 2007. Low temperature preparation and visible light photocatalytic activity of mesoporous carbon-doped crystalline TiO2. *Appl Catal B* 69(3-4): 138-144. https://doi.org/10.1016/j.apcatb.2006.06.015
22. Robel I, Subramanian V, Kuno M, Kamat PV. 2006. Quantum dot solar cells harvesting light energy with CdSe nanocrystals molecularly linked to mesoscopic TiO2 films. *J Am Chem Soc* 128(7): 2385-2393. https://doi.org/10.1021/ja056494n
23. Frank SN, Bard AJ. 1977. Heterogeneous photocatalytic oxidation of cyanide ion in aqueous solutions at titanium dioxide powder. *J Am Chem Soc* 99(1): 303-304. https://doi.org/10.1021/ja00443a081
24. Vinodgopal K, Kamat PV. 1995. Enhanced rates of photocatalytic degradation of an azo dye using SnO2/TiO2 coupled semiconductor thin films. *Environ Sci Technol* 29(3): 841-845. https://doi.org/10.1021/es00003a037
25. Miyauchi M, Nakajima A, Watanabe T, Hashimoto K. 2002. Photoinduced hydrophilic conversion of TiO2/WO3 layered thin films. *Chem Mater* 14(11): 4714-4720. https://doi.org/10.1021/cm020355c
26. Kang X, Liu S, Dai Z, He Y, Song X, et al. 2019. Titanium dioxide: Form engineering to application. *Catalysts* 9(2): 191. https://doi.org/10.3390/catal9020191
27. Lu Y, Guan S, Hao L, Yoshida H. 2015. Review on the photocatalyst coatings of TiO2: fabrication by mechanical coating technique and its application. *Coatings* 5(3): 425-464. https://doi.org/10.3390/coatings5030425
28. Yoshida H, Lu Y, Nakayama H, Hirohashi M. 2009. Fabrication of TiO2 film by mechanical coating technique and its photocatalytic activity. *J Alloys Compd* 475(1-2): 383-386. https://doi.org/10.1016/j.jallcom.2008.07.059
29. Guan S, Hao L, Yoshida H, Asanuma H, Pan F, et al. 2015. Influence of carbon atmosphere on surface morphology and photocatalytic activity of TiO2 coatings by multi-heat treatment. *J Mater Sci: Mater Electron* 27: 3873-3879. https://doi.org/10.1007/s10854-015-4236-0
30. Spuur RA, Myers H. 1957. Quantitative analysis of anatase-rutile mixtures with an X-ray diffractometer *Anal Chem* 29(5): 760-762. https://doi.org/10.1021/ac60125a006
31. Zhang H, Banfield JF. 2000. Understanding polymorphic phase transformation behavior during growth of nanocrystalline aggregates: Insights from TiO2. *J Phys Chem B* 104(15): 3481-3487. https://doi.org/10.1021/jp000499j
32. Zhang J, Xu Q, Li M, Feng Z, Li C. 2009. UV raman spectroscopic study on TiO2. II. Effect of nanoparticle size on the outer/inner phase transformation. *J Phys Chem C* 113(5): 1698-1704. https://doi.org/10.1021/jp808013k
33. Sun P, Liu HB, Yang HB, Fu WY, Liu SK, et al. 2010. Synthesis and characterization of TiO2 thin films coated on metal substrate. *Appl Surf Sci* 256(10): 3170-3173. https://doi.org/10.1016/j.apsusc.2009.11.093
34. Xu MW, Bao SJ, Zhang XG. 2005. Enhanced photocatalytic activity of magnetic TiO2 photocatalyst by silver deposition. *Materials Letters* 59(17): 2194-2198. https://doi.org/10.1016/j.matlet.2005.02.065

35. Lu Y, Matsuzaka K, Hao L, Hirakawa Y, Yoshida H, et al. 2013. Photocatalytic activity of TiO2/Ti composite coatings fabricated by mechanical coating technique and subsequent heat oxidation. *Mater Sci Semicond Process* 16(6): 1949-1965. https://doi.org/10.1016/j.mssp.2013.07.024

36. Chen X, Mao SS. 2007. Titanium dioxide nanomaterials: synthesis, properties, modifications, and applications. *Chem Rev* 107(7): 2891-2959. https://doi.org/10.1021/cr0500535

37. Chen D, Ye JH. 2009. Selective-synthesis of high-performance single-crystalline Sr2Nb2O7 nanoribbon and SrNb2O6 nanorod photocatalysts. *Chem Mater* 21(11): 2327-2333. https://doi.org/10.1021/cm8034714

38. Li Q, Yue B, Iwai H, Kako T, Ye J. 2010. Carbon nitride polymers sensitized with N-doped tantalic acid for visible light-induced photocatalytic hydrogen evolution. *J Phys Chem C* 114(9): 4100-4105. https://doi.org/10.1021/jp911803z

39. Tong H, Ouyang S, Bi Y, Umezawa N, Oshikiri M, et al. Nano-photocatalytic materials: possibilities and challenges. *Adv Mater* 24(2): 229-251. https://doi.org/10.1002/adma.201102752

40. Nakata K, Fujishima A. 2012. TiO2 photocatalysis: design and application. *J Photochem Photobiol C Photochem Rev* 13(3): 169-189. https://doi.org/10.1016/j.jphotochemrev.2012.06.001

41. Xu C, Anusuyadevi PR, Aymonier C, Luque R, Marre S. 2019. Nanostructured materials for photocatalysis. *Chem Soc Rev* 48(14): 3868-3902. https://doi.org/10.1039/C9CS00102F

42. Gao B, Sun M, Ding W, Ding Z, Liu W. 2021. Decoration of γ-graphyne on TiO2 nanotube arrays: improved photoelectrochemical and photoelectrocatalytic properties. *Appl Catal B* 281: 119492. https://doi.org/10.1016/j.apcatb.2020.119492

43. Joo JB, Lee I, Dahl M, Moon GD, Zaera F, et al. 2013. Controllable synthesis of mesoporous TiO2 hollow shells: toward an efficient photocatalyst. *Adv Funct Mater* 23(34): 4246-4254. https://doi.org/10.1002/adfm.201300255

44. Xia Y, Li F, Jiang Y, Xia M, Xue B, et al. 2014. Interface actions between TiO2 and porous diatomite on the structure and photocatalytic activity of TiO2-diatomite. *Appl Surf Sci* 303: 290-296. https://doi.org/10.1016/j.apsusc.2014.02.169

45. Mamaghani AH, Haghighat F, Lee CS. 2019. Photocatalytic oxidation of MEK over hierarchical TiO2 catalysts: effect of photocatalyst features and operating conditions. *Appl Catal B* 251: 1-16. https://doi.org/10.1016/j.apcatb.2019.03.057

46. Yan M, Chen F, Zhang J, Anpo M. 2005. Preparation of controllable crystalline titania and study on the photocatalytic properties. *J Phys Chem B* 109(18): 8673-8678. https://doi.org/10.1021/jp046087i

47. Zheng W, Liu X, Yan Z, Zhu L. 2009. Ionic liquid-assisted synthesis of large-scale TiO2 nanoparticles with controllable phase by hydrolysis of TiCl4. *ACS Nano* 3(1): 115-22. https://doi.org/10.1021/nn800713w

48. Hao L, Guan S, Takaya S, Hiroyuki Y, et al. 2017. Preparation of visible-light-responsive TiO2 coatings using molten KNO3 treatment and their photocatalytic activity. *Appl Surf Sci* 407: 276-281. https://doi.org/10.1016/j.apsusc.2017.02.097

49. Ma H, Yang J, Dai Y, Zhang Y, Lu B, et al. 2007. Raman study of phase transformation of TiO2 rutile single crystal irradiated by infrared femtosecond laser. *Appl Surf Sci* 253(18): 7497-7500. https://doi.org/10.1016/j.apsusc.2007.03.047

50. Ilie AG, Scarisoareanu M, Morjan I, Dutu E, Badiceanu M, et al. 2017. Principal component analysis of Raman spectra for TiO2 nanoparticle characterization. *Appl Surf Sci* 417: 93-103. https://doi.org/10.1016/j.apsusc.2017.01.193

51. Xia X, Peng S, Bao Y, Wang Y, Lei B, et al. 2018. Control of interface between anatase TiO2 nanoparticles and rutile TiO2 nanorods for efficient photocatalytic H2 generation. *J Power Sources* 376: 11-17. https://doi.org/10.1016/j.jpowsour.2017.11.067

52. Preethi LK, Mathews T, Nand M, Jha SN, Gopinath CS, et al. 2017. Band alignment and charge transfer pathway in three phase anatase-rutile-brookite TiO2 nano-tubes: an efficient photocatalyst for water splitting. *Appl Catal B* 218: 9-19. https://doi.org/10.1016/j.apcatb.2017.06.033

53. Guan S, Hao L, Yoshida H, Pan F, Asanuma H, et al. 2017. Black composites photocatalyst coatings of K2Ti6O13-TiO2/TiC with nano-sheet flower-like structure by heat treatment in molten salt. *Materials Letters* 188: 55-58. https://doi.org/10.1016/j.matlet.2016.10.092

54. Fei J, Li J. 2015. Controlled preparation of porous TiO2-Ag nanostructures through supramolecular assembly for plasmon-enhanced photocatalysis. *Adv Mater* 27(2): 314-319. https://doi.org/10.1002/adma.201404007

55. Ding Y, Zhou L, Mo L, Jiang L, Hu L, et al. 2015. TiO2 microspheres with controllable surface area and porosity for enhanced light harvesting and electrolyte diffusion in dye-sensitized solar cells. *Adv Funct Mater* 25(37): 5946-5953. https://doi.org/10.1002/adfm.201502224

56. Nie L, Yu J, Li X, Cheng B, Liu G, et al. 2013. Enhanced performance of NaOH-modified Pt/TiO2 toward room temperature selective oxidation of formaldehyde. *Environ Sci Technol* 47(6): 2777-2783. https://doi.org/10.1021/es3045949

57. Ning X, Liu H, Zhu H. 2010. Anodic dissolution behavior of TiCxOy in NaCl-KCl melt. *Electrochemistry* 78: 513-516.

58. Khan SUM, Al-Shahry M, William BI. 2002. Efficient photochemical water splitting by a chemically modified n-TiO2. *Science* 297(5590): 2243-2245. https://doi.org/10.1126/science.1075035

59. Dvoranova D, Brezova V, Mazur M, Malati MA. 2002. Investigations of metal-doped titanium dioxide photocatalysts. *Appl Catal B* 37(2): 91-105. https://doi.org/10.1016/S0926-3373(01)00335-6

60. Diwald O, Thompshon TL, Zubkov T, Goralski EG, Walck SD, et al. 2004. Photochemical activity of nitrogen-doped rutile TiO2 (110) in visible light. *J Phys Chem B* 108(19): 6004-6008. https://doi.org/10.1021/jp031267y

61. Dong F, Wang H, Wu Z. 2009. One-step "Green" synthetic approach for mesoporous C-doped titanium dioxide with efficient visible light photocatalytic activity. *J Phys Chem C* 113(38): 16717-16717. https://doi.org/10.1021/jp9049654

62. Barborini E, Conti AM, Kholmanov IN, Miseri P, Podesta A, et al. 2005. Nanostructured TiO2 films with 2 eV optical gap. *Adv Mater* 17(15): 1842-1846. https://doi.org/10.1002/adma.200401169

63. Peng X, Chen A. 2004. Aligned TiO2 nanorod arrays synthesized by oxidizing titanium with acetone. *J Mater Chem* 14: 2542-2548. https://doi.org/10.1039/B404750H

64. Gracia F, Holgado JP, Contreras L, Girardeau T, Gonzalez-Elipe AR. 2003. Optical and crystallisation behaviour of TiO2 and V/TiO2 thin films prepared by plasma and ion beam assisted methods. *Thin Solid Films* 429(1-2): 84-90. https://doi.org/10.1016/S0040-6090(03)00431-0

65. Chen CH, Shieh J, Hsieh SM, Kuo CL, Liao HY. 2012. Architecture, optical absorption, and photocurrent response of oxygen-deficient mixed-phase titania nanostructures. *Acta Mater* 60(18): 6429-6439. https://doi.org/10.1016/j.actamat.2012.08.030

66. K Huang, Y Li, Xing Y. 2013. Carbothermal synthesis of titanium oxycarbide as electrocatalyst support with high oxygen evolution reaction activity. *J Mater Res* 28: 454-460. https://doi.org/10.1557/jmr.2012.353

67. Jiao S, Ning X, Huang K, Zhu H. 2010. Electrochemical dissolution behavior of conductive TiCxO1–x solid solutions. *Pure Appl Chem* 82(8): 1691-1699. https://doi.org/10.1351/PAC-CON-09-10-39

68. Rudiger C, Maglia F, Leonardi S, Sachsenhauser M, Sharp I, et al. 2012. Surface analytical study of carbothermally reduced titania films for electrocatalysis application. *Electrochim Acta* 71: 1-9. https://doi.org/10.1016/j.electacta.2012.02.044

69. Irie H, Watanabe Y, Hashimoto K. 2003. Carbon-doped anatase TiO2 powders as a visible-light sensitive photocatalyst. *Chem Lett* 32(8): 772-773.

70. Guan S, Hao L, Lu Y, Yoshida H, Pan F, et al. 2016. Fabrication of oxygen-deficient TiO2 coatings with nano-fiber morphology for visible-light photocatalysis. *Mater Sci Semicond Process* 41: 358-363. https://doi.org/10.1016/j.mssp.2015.09.018

71. Chen X, Shen S, Guo L, Mao S. 2010. Semiconductor-based photocatalytic hydrogen generation. *Chem Rev* 110(11): 6503-6570. https://doi.org/10.1021/cr1001645

72. Wang H, Zhang L, Chen Z, Hu J, Li S, et al. 2014. Semiconductor heterojunction photocatalysts: design, construction, and photocatalytic performances. *Chem Soc Rev* 43: 5234-5244. https://doi.org/10.1039/C4CS00126E

73. Ignaszak A, Song C, Zhu W, Zhang J, Bauer A, et al. 2012. Titanium carbide and its core-shelled derivative TiC@TiO2 as catalyst supports for proton exchange membrane fuel cells. *Electrochim Acta* 69: 397-405. https://doi.org/10.1016/j.electacta.2012.03.039

74. Li Y, Ishigaki T. 2003. Core-shell micron-scale composites of titanium oxide and carbide formed through controlled thermal-plasma oxidation. *Chem Phys Lett* 367(5-6): 561-565. https://doi.org/10.1016/S0009-2614(02)01760-8

75. Stott JS, Mortimer RJ, Dann SE, Oyama M, Marken F. 2006. Electrochemical properties of core-shell TiC-TiO2 nanoparticle films immobilized at ITO electrode surfaces. *Phys Chem Chem Phys* 8: 5437-5443. https://doi.org/10.1039/B610391J

76. Diebold U. 2003. The surface science of titanium dioxide. *Surf Sci Rep* 48(5-8): 53-229. https://doi.org/10.1016/S0167-5729(02)00100-0

77. Oshima C, Otani S, Aono M, Zaima S, Shibata Y. 1983. Titanium oxycarbide on TiC (100) surface. *Jpn J Appl Phys* 22(6R): 930-933.

78. Bellucci A, Gozzi D, Nardone M, Sodo A. 2003. Rutile growth mechanism on TiC monocrstals by oxidation. *Chem Mater* 15(5): 1217-1224. https://doi.org/10.1021/cm021204c

79. Zhang X, Chen Z. 2015. Enhanced photoelectrochemical performance of the hierarchical micro/nano-structured TiO2 mesoporous spheres with oxygen vacancies via hydrogenation. *RSC Adv* 5: 9482-9488. https://doi.org/10.1039/C4RA13300E

80. Setvin M, Aschauer U, Scheiber P, Li YF, Hou W, et al. 2013. Reaction of O2 with subsurface oxygen vacancies on TiO2 anatase (101). *Science* 341(6149): 988-991. https://doi.org/10.1126/science.1239879

81. Zhang X, Qin J, Xue Y, Yu P, Zhang B, et al. 2014. Effect of aspect ratio and surface defects on the photocatalytic activity of ZnO nanorods. *Sci Rep* 4: 4596. https://doi.org/10.1038/srep04596

82. Gharagozlou M, Bayati R. 2014. Photocatalytic activity and formation of oxygen vacancies in cation doped anatase TiO2 nanoparticles. *Ceram* 40(7 Part B): 10247-10253. https://doi.org/10.1016/j.ceramint.2014.02.114

83. Cong Y, Zhang J, Chen F, Anpo M. 2007. Synthesis and characterization of nitrogen-doped TiO2 nanophotocatalyst with high visible light activity. *J Phys Chem C* 111(19): 6976-6982. https://doi.org/10.1021/jp0685030

84. Vanheusden K, Seager CH, Warren WL, Tallant DR, Voigt JA. 1998. Correlation between photoluminescence and oxygen vacancies in ZnO phosphors. *Appl Phys Lett* 68(3): 403-405. https://doi.org/10.1063/1.116699

85. Das J, Mishra DK, Srinivasu VV, Sahu DR, Roul BK. 2015. Photoluminescence and Raman studies for the confirmation of oxygen vacancies to induce ferromagnetism in Fe doped Mn: ZnO compound. *J Magn Magn Mater* 382: 111-116. https://doi.org/10.1016/j.jmmm.2015.01.058

86. Su J, Geng P, Li X, Zhao Q, Quan X, et al. 2015. Novel phosphorus doped carbon nitride modified TiO2 nanotube arrays with improved photoelectrochemical performance. *Nanoscale* 7: 16282-16289. https://doi.org/10.1039/C5NR04562B

87. Su J, Zhu L, Chen G. 2016. Ultrasmall graphitic carbon nitride quantum dots decorated self-organized TiO2 nanotube arrays with highly efficient photoelectrochemical activity. *Appl Catal B* 186: 127-135. https://doi.org/10.1016/j.apcatb.2015.12.050

88. Zhu X, Wang Y, Qin W, Zhang S, Zhou D. 2016. Distribution of free radicals and intermediates during the photodegradation of polychlorinated biphenyls strongly affected by cosolvents and TiO2 catalyst. *Chemospere* 144: 628-634. https://doi.org/10.1016/j.chemosphere.2015.09.039

89. Shi J, Liu C, He C, Li J, Xie C, et al. 2015. Carbon-doped titania nanoplates with exposed {001} facets: Facile synthesis, characterization and visible-light photocatalytic performance. *RSC Adv* 5: 17667-17675. https://doi.org/10.1039/C4RA15824E

90. Guan S, Hao L, Yoshida H, Pan F, Asanuma H, et al. 2016. Enhanced photocatalytic activity of photocatalyst coatings by heat treatment in carbon atmosphere. *Materials Letters* 167: 43-46. https://doi.org/10.1016/j.matlet.2015.12.074

91. Tachibana Y, Vayssieres L, Durant JR. 2012. Artificial photosynthesis for solar water-splitting. *Nat Photonics* 6: 511-518. https://doi.org/10.1038/nphoton.2012.175

92. Kiran V, Sampath S. 2012. Enhanced Raman spectroscopy of molecules adsorbed on carbon-doped TiO2 obtained from titanium carbide: A visible-light-assisted renewable substrate. *ACS Appl Mater Interfaces* 4(8): 3818-3828. https://doi.org/10.1021/am300349k

93. Chen C, Cai W, Long M, Zhou B, Wu Y, et al. 2010. Synthesis of visible-light responsive graphene oxide/TiO2 composites with p/n heterojunction. *ACS Nano* 4(11): 6425-6432. https://doi.org/10.1021/nn102130m

94. Liu J, Bai H, Wang Y, Liu Z, Zhang X, et al. 2010. Self-assembling TiO2 nanorods on large graphene oxide sheets at a two-phase interface and their anti-recombination in photocatalytic applications. *Adv Funct Mater* 20(23): 4175-4181. https://doi.org/10.1002/adfm.201001391

95. Wei X, Cao J, Fang F. 2018. A novel multifunctional Ag and Sr2+ co-doped TiO2@rGO ternary nanocomposite with enhanced p-nitrophenol degradation, and bactericidal and hydrogen evolution activity. *RSC Adv* 8: 31822-31829. https://doi.org/10.1039/C8RA06813E